University of Belgrade
Faculty of Physics

Master Thesis

Holographic Square Lattices and Strange Metals

Author:
Vladan Gecin

Supervisor:
Dr. Mihailo Čubrović

September, 2022
Belgrade

Univerzitet u Beogradu
Fizički fakultet

Master rad

Holografske kvadratne rešetke i čudni metali

Autor:
Vladan Gecin

Mentor:
Dr Mihailo Čubrović

Septembar, 2022.
Beograd

Abstract

Strange metals still resist a comprehensive theoretical description. Yet, the AdS/CFT correspondence (holographic principle) provides a novel, nonperturbative insight into the properties of these strongly correlated materials by constructing a theory with gravity, which is dual (equivalent) to the starting field-theoretical (condensed matter) problem. In this thesis we find the numerical solution to a system of Einstein-Maxwell-dilaton equations with periodic boundary conditions, which describes strongly correlated matter at finite temperature and chemical potential on a square lattice. The metric in the deep interior of the AdS space is hyperscaling-violating, implying an anomalous scaling of thermodynamic quantities. We then compute the charge density of the system and inspect the validity of the Luttinger theorem. The theorem is strongly violated, meaning that the system is a non-Fermi liquid, as expected. We test our numerical method in detail and show that it provides a robust framework for further work.

Sažetak

Potpun teorijski opis čudnih metala još uvek nije postignut. Ipak, AdS/CFT korespondencija (holografski princip) pruža nov, neperturbativni uvid u osobine ovih jako korelisanih materijala opisom koji uključuje i gravitaciju, a koji je dualan (ekvivalentan) početnom problemu u teoriji polja (specijalno, u okviru fizike kondenzovane materije). U ovom radu su nađena numerička rešenja Ajnštajn-Maksvel-dilatonskih jednačina sa periodičnim graničnim uslovima koja opisuju jako korelisanu materiju na konačnoj temperaturi i konačnom hemijskom potencijalu, na kvadratnoj rešetki. Dobijena metrika u unutrašnjosti AdS prostora narušava hiperskaliranje, ukazujući na anomalno skaliranje termodinamičkih veličina. Za dati sistem izračunata je potom gustina naelektrisanja, uz proveru primenljivosti Latindžerove teoreme. Teorema u ovom sistemu ne važi, pa je sistem ne-Fermijeva tečnost, kao što se i očekuje. Numeričke metode su pritom detaljno testirane, uz zaključak da korišćena numerika predstavlja dobru osnovu za dalji rad.

Acknowledgements

I would like to thank my supervisor Dr. Mihailo Čubrović for exceptional enthusiasm, dedication and patience he has shown in the course of our collaboration. His guidance in this research was invaluable, and I am deeply grateful for all the knowledge he has shared with me. I am grateful for his lectures, suggestions, and selfless devotion to the refining of my ideas and writing, as well as for being always available for discussion and ready to help.

Also, I thank the factory "Teleoptik-Gyroscopes" (where I was employed during my master's studies), along with my former colleagues from the Optical Laboratory, for the privileges they gave to me in order to support and encourage my education.

Finally, I would like to thank my family and friends, for without their help and support in realization of my goals these lines might have never been written.

Contents

Chapter 1

Strange metals and holography: motivation

Since 1980s physicists have gathered a vast amount of experimental data introducing novel phases of matter with metallic properties that cannot be comprehended by the means of conventional theoretical apparatus. Perhaps the most intriguing are the *strange metals* (SM). All previously known metallic states were either successfully described by Landau's theory of Fermi liquids or else they were known to break some symmetry (i.e. magnetic materials). Strange metals exhibit a phenomenology which is completely different from normal metals and yet they do not manifestly break any symmetry. Their behavior has turned out to resist any adequate theoretical explanation.

The Fermi liquid (FL) theory [1, 2] is built, roughly speaking, on two cornerstones. It postulates the existence of a Fermi surface (FS) and assumes a description of the system in terms of stable weakly interacting low-energy elementary excitations with respect to the Fermi level. These excitations – *the quasiparticles* – have a dispersion relation similar to that of a nearly free Fermi gas, with effective parameters (mass, Fermi velocity, etc.) which contain all the information on the (possibly strong) interactions among the constituent fermions. Their decay rate scales universally as $\Gamma \sim \omega^2$, confirming that the excitations are long-lived (underdamped).

On the other hand, non-Fermi liquids may have neither a sharp Fermi surface nor well defined quasiparticles. Still, their behavior should not be viewed as contrasting to that of Fermi liquids, but rather as a set of complementary phenomena. Thus, we define the FS as a locus of points in momentum space where the spectral weight is non-analytic at $\omega = 0$, in accordance with FL theory where it is determined by the pole of the propagator [3]. Experimentally, such a pole manifests as a sharp peak obtained in Angular Resolved Photoemission Spectroscopy (ARPES) measurements. In the ARPES experiments electrons are knocked out from the sample due to the photoelectric effect and the intensity of the resulting electron beam is measured under different angles. Since the intensity of an electron beam $I(\omega, \mathbf{k}) \propto n_F(\omega, \mathbf{k}) A(\omega, \mathbf{k})$, where $n_F(\omega, \mathbf{k})$ and $A(\omega, \mathbf{k}) \propto \mathrm{Im} G_R(\omega, \mathbf{k})$ are respectively the Fermi-Dirac distribution and the electron spectral function, the occupancy of the Fermi level is naturally reflected as a non-analyticity of the Green's function [3]. In the case of a non-Fermi liquid such peaks may drastically widen, and their width determines the decay rate and lifetime of the excitations near the FS. In many cases it can be parametrized as $\Gamma \sim \omega^{2\nu}$, where ν can take any real or even complex value [2].

Thus, we already anticipate the versatility of states comprised by the term "strange metal". Generally, these states show scaling laws, so they may properly be called *quan-*

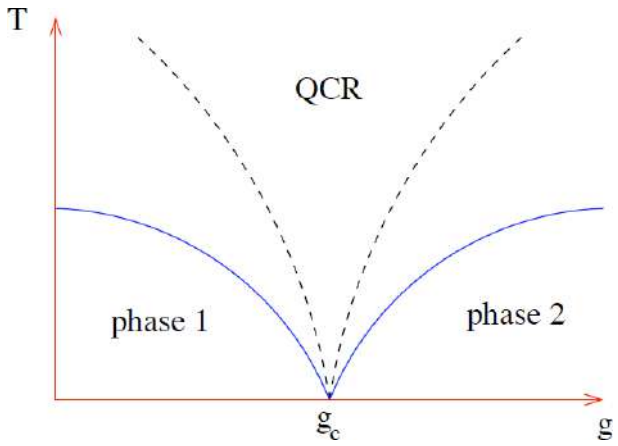

Figure 1.1: Quantum criticality: blue lines separate different ordered phases emerging upon decrease in temperature for a given parameter g, while g_c determines a zero-temperature second-order quantum phase transition between these phases; it is a QCP. The QCR then arises at the intersection of the blue lines and spreads between the dashed lines. Adapted from [5].

tum critical states [4]. The simplest way for a quantum critical behavior to emerge is the *quantum critical point* (QCP). It is a point at $T = 0$ where a second-order quantum phase transition occurs upon a continuous change of some control parameter. The *quantum critical regime* (QCR) then arises above the QCP as one increases the temperature (Figure 1.1).

A famous and well-supported example of a QCP is found in heavy fermion[1] systems, which have a normal (heavy) Fermi liquid phase and a non-Fermi-liquid phase, separated by a quantum critical point; on top of that, there is usually also an antiferromagnetic (AF) critical point [6, 7]. Another important manifestation of quantum criticality is linked to cuprate[2] high-T_c superconductors, with the exception that the QCP naturally does not exist, since the superconducting phase covers the region where the QCP is expected to be (Figure 1.2). A similar example is offered by pnictide[3] high-T_c superconductors (Figure 1.3) [4].

Nevertheless, a QCP may be reached in cuprates if superconductivity is suppressed by a strong magnetic field, although it is more likely that one gets a zero-temperature SM phase [4, 8]. Indeed, one should be aware that quantum critical behavior sometimes spreads across a finite interval of parameters (at $T = 0$), so that instead of a point a *quantum critical phase* emerges, and the best candidate for a quantum critical phase is precisely the SM phase of the cuprate superconductors (the transparent region between the dopings n_{FSR} and n_c on Figure 1.2).

In contrast to the great diversity of the ordered (symmetry-broken) phases, the strange metals are quite robust and share some key common properties. One of their hallmarks is the resistivity which is linear in temperature T, unlike the quadratic dependence of

[1]Heavy fermions are quasiparticles that emerge due to the Kondo interaction between strongly correlated f-electrons and the electrons in a conduction band. Their effective mass exceeds the electron mass up to a hundred times, leading to the attribute "heavy".

[2]Cuprates are compounds with alternating layers of conducting copper-oxide and some insulating doped metal oxide, which serves as electron/hole reservoir.

[3]Pnictides are binary compounds of the elements in the fifteenth group of the periodic table.

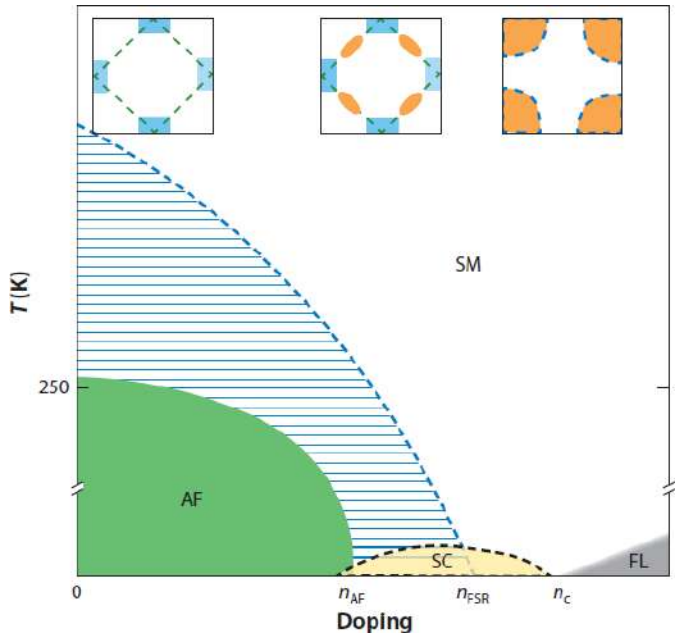

Figure 1.2: A schematic phase diagram of electron-doped cuprates with two-dimensional Fermi surfaces for various doping regions. Adapted from [8].

an ordinary metal [9]. Such a scaling usually spreads from a very low[4] T up to the very high temperatures (even to the melting point), violating the Mott-Ioffe-Regel (MIR) limit. This limit is reached when the mean free path becomes equal to the lattice constant. For quasiparticle-based transport, it manifests as the saturation of the resistivity. Its violation clearly indicates that coherent quasiparticles are not the correct degrees of freedom. Metals that do not saturate at the MIR limit are called "bad metals". However, unlike the true bad metals, the strange metals have very low resistivity at low T. As an illustration, on Figure 1.3 we show the temperature dependence of the resistivity of a pnictide – in the red region it is linear, indicating a strange metal [4, 9].

The phenomenology considered above plus the absence of a conventional field-theoretical explanation hint at some deep and universal underlying physics. Certainly, strange metal phases emerge from strongly correlated materials. A prototype example of a Hamiltonian which exhibits strongly coupled physics, and yet is quite simple and intuitive to write down, is the Hubbard model [10]

$$H = -t \sum_{\langle i,\, j\rangle} \sum_{\sigma} \left(c^{\dagger}_{i\sigma} c_{j\sigma} + c^{\dagger}_{j\sigma} c_{i\sigma} \right) + \sum_{i} \left(U n_{i\uparrow} n_{i\downarrow} - \mu (n_{i\uparrow} + n_{i\downarrow}) \right). \tag{1.1}$$

The strong on-site Coulomb interaction between the electrons (U) makes the Hubbard Hamiltonian resistant to the usual perturbative methods of quantum field theory. Still, a few approaches may give satisfactory results:

- Exact diagonalization (ED) – this is certainly the most accurate and straightforward method, which does not involve any additional physical assumptions, but it works well only for small lattices [11].

[4] In fact – from the critical temperature where superconductivity kicks in. Extrapolations predict that the strange-metallic dependence goes all the way down to $T = 0$, but that is impossible to check experimentally.

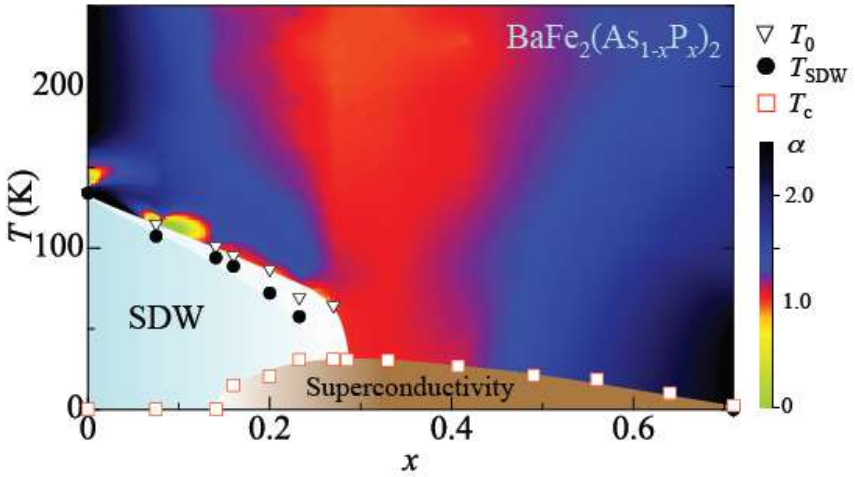

Figure 1.3: The phase diagram for $BaFe_2(As_{1-x}P_x)_2$ with doping x and the temperature exponent of the resistivity α. SDW denotes the spin density waves, the excitations of the antiferromagnetic phase. Adapted from [4].

- Quantum Monte Carlo (QMC) – a numerical algorithm based on random sampling of the path integral configurations when computing the partition function and its functional derivatives (i.e. correlation functions). It does not attempt to find an exact solution, so for larger systems it works better than exact diagonalization (although it still does not admit very large lattices). However, QMC suffers from the fermion sign problem – the terms in the partition function are not positive definite due to the antisymmetrization of the fermionic wave-function, so the convergence is very slow and we are limited to relatively high temperatures [11, 12].

- Dynamical mean-field theory (DMFT) – maps the lattice problem to a one-site interaction with an "electron bath", i.e. to the Anderson impurity model. It works at low temperatures, but its setup involves many assumptions. Also, its efficiency increases with coordination number, i.e. with the dimensionality of the lattice. Therefore, it becomes exact when the number of spatial dimensions is infinite [13, 14].

- Dynamical cluster approximation (DCA) – solves a QMC problem on a small lattice which interacts with an electron bath. It is a variation on DMFT, which also works well at low temperatures [15].

Unfortunately, none of these methods allows us to obtain the solution in a controlled manner: we still need an adequate tool for dealing with strongly coupled field theories in a predictable way. A natural candidate is thus the AdS/CFT correspondence, i.e. the holographic duality [16, 17, 18]. It is a *weak-strong duality* developed within string theory, which can establish the equivalence between a weakly coupled semiclassical theory with gravity and a strongly coupled conformal field theory, offering thereby the means for describing strongly correlated systems in terms of general relativity. Although such field theories resemble the condensed matter systems only in their main features, the AdS/CFT correspondence undoubtedly helps us to make a step forward in calculating thermodynamic potentials and correlation functions for strongly correlated materials.

Despite being promising, the application of the AdS/CFT correspondence in condensed matter physics, often called "AdS/CMT", is still a young field. Its main success so far

is the determination of various response functions and the description of some condensed matter systems in terms of an effective field theory [19, 15]. Yet, what is genuinely novel are recent attempts at enhancing the holographic models by inclusion of an ionic lattice. Such attempts are still few and far apart, and almost all pertain to one-dimensional chains. A two-dimensional lattice is rarely studied, and no one has ever computed either a response or correlation function in such a background. This is so because the construction of 2D lattices calls for solving the Einstein-Maxwell-dilaton (EMD) equations with oscillatory boundary conditions, which poses one of the most difficult static problems in numerical relativity.

In that regard, we expand the field of AdS/CMT. Indeed, our goal is to construct a holographic square lattice by the means of varying chemical potential and to probe the strange-metallic nature of the system from the perspective of the Luttinger theorem. In order to access the strongly coupled field theory and determine the corresponding electric charge density, we solve the EMD equations.

Since the AdS/CFT correspondence calls for an interdisciplinary approach and involves both high- and low-energy physics, we have dedicated a large portion of the thesis to the explanation of the formalism and its usage: in the next chapter we lay the foundations for holographic duality, and consequently, in chapter 3, we explain the principles of its application in condensed matter physics. The rest of the thesis brings the discussion of our original results. Namely:

1. we have constructed an ionic 2D holographic lattice (chapter 4) and these results were used in the first study of fermionic spectra in such a background: F. Herček, V. Gecin and M. Čubrović, Photoemission "experiments" on holographic lattices, arXiv:2208.05920 [20];

2. in particular, we have found the analytical solution to the EMD equations with lattice symmetry in the vicinity of an arbitrary-temperature horizon and we have proved that the lattice corrections to the metric are indeed irrelevant in the near-horizon region [21, 20] (chapter 4);

3. we have found that this "IR solution" may be extended all the way to the "UV region" near the AdS boundary (chapter 5);

4. we have determined the gauge and dilaton fields solving the subset of the EMD equations (chapter 5);

5. we have computed the electric charge density and tested the validity of the Luttinger theorem [22, 23] (chapter 6).

Chapter 2

The formalism of AdS/CFT

2.1 Theoretical framework

In this section we are going to examine a few key theoretical concepts underlying the holographic duality (AdS/CFT correspondence, gauge/gravity duality). These tools are essential both for the rigorous string-theoretical approach ("top-down") and for its condensed matter applications, which typically consider phenomenological backgrounds, not those obtained from string theory ("bottom-up").

2.1.1 Anti-de Sitter space-time (AdS)

AdS_{d+2} space-time is a $(d+2)$-dimensional maximally symmetric solution of the Einstein equations, with d being the number of space dimensions on its boundary.[1] The term *maximally symmetric* refers to the fact that such spaces have the maximal number of Killing vectors (which equals the number of the independent components of the metric). Consequently, symmetry constrains the form of the Riemann tensor for such a space, because it cannot depend on derivatives of the metric. Therefore we postulate:

$$R_{\mu\nu\rho\sigma} = C(g_{\mu\rho}g_{\nu\sigma} - g_{\mu\sigma}g_{\nu\rho}). \tag{2.1}$$

Contracting (2.1) twice and using the Biancchi identity, it is easy to show that C is a constant. Solving the Einstein equations with $\Lambda < 0$ we get

$$R = \frac{2(d+2)}{d}\Lambda. \tag{2.2}$$

This space-time has a negative curvature and corresponds to the Lorentzian generalization of a hyperboloid. Its isometry group is $\mathrm{SO}(2,\, d+1)$.

If we define

$$\Lambda = -\frac{d(d+1)}{2L^2}, \tag{2.3}$$

AdS_{d+2} space-time may be viewed as a $(d+2)$-dimensional hypersurface

$$-X_{-1}^2 - X_0^2 + \sum_{i=1}^{d+1} X_i^2 = -L^2, \tag{2.4}$$

[1] This convention is going to be more clear in the sections to come.

embedded in a $(d+3)$-dimensional Minkowski space with two time directions. The positive constant L is called the *AdS radius*.[2] If we transform the coordinates as $X_{-1} = L\cosh\rho\cos\tau$, $X_0 = L\cosh\rho\sin\tau$ and $X_i = L\sinh\rho\, x_i$, with $\rho \in [0,\,\infty)$, $\tau \in [0,\,2\pi]$ and $\sum_{i=1}^{d+1} x_i^2 = 1$, we find the induced metric on the embedding (2.4):

$$ds^2 = L^2\left(d\rho^2 - \cosh^2\rho\, d\tau^2 + \sinh^2\rho\, d\Omega_d^2\right). \tag{2.5}$$

Extending τ to the whole real axis recovers the universal cover of AdS_{d+2} in *global coordinates*. Defining $\sinh\rho = \tan\varphi$, with $\varphi \in [0,\,2\pi]$, it may be shown that AdS_{d+2} is topologically equivalent to a cylinder with a d-sphere at each point [15, 24].

On the other hand, the coordinate transformation $X_0 = Lt/z$, $X_i = Lx_i/z$ $(i = 1,\ldots,d)$ and $X_{\theta(\pm1)d\pm1} = (L^2 \mp z^2 \pm t^2 \mp \sum_{i=1}^{d} x_i^2)/(2z)$, with $t, x_i \in \mathbb{R}$ and $z \in (0,\,\infty)$ being the inverse of the radial coordinate r, gives us a portion of this cylinder, a chart called *Poincaré patch*. Its metric is

$$ds^2 = \frac{L^2}{z^2}\left(-dt^2 + dz^2 + \sum_{i=1}^{d} dx_i^2\right). \tag{2.6}$$

We will find the Poincaré patch convenient because in these coordinates the AdS boundary $(z = 0)$ is a Minkowski space-time [15].

2.1.2 Conformal field theory (CFT)

The isometries of an AdS space-time exhibit conformal invariance near its boundary [24]. Such a symmetry suggests that a link between the physics at the AdS boundary and conformal field theory might be established. We will explore this connection in section 2.2 in detail, but we first discuss the basic properties of CFTs.

A diffeomorfism ϕ between manifolds $(\mathcal{M},\, g)$ and $(\mathcal{N},\, g')$ is said to be a *conformal* map if there exists a smooth map Ω on $\mathcal{M}$, called *conformal factor*, such that $\phi^* g' = \Omega^2\, g$. Writing out explicitly the coordinate dependence, we get [25]

$$g'_{\rho\sigma}(x')\frac{\partial x'^{\rho}}{\partial x^{\mu}}\frac{\partial x'^{\sigma}}{\partial x^{\nu}} = \Omega^2(x) g_{\mu\nu}(x). \tag{2.7}$$

We see that conformal map preserves angles. Substituting an infinitesimal transformation $x' = x + \zeta(x)$ in (2.7) and considering the Minkowski metric η in $d+1$ dimensions, we easily find the *conformal Killing equation:*

$$\partial_{(\mu}\zeta_{\nu)} = \frac{1}{d+1}(\partial^{\rho}\zeta_{\rho})\eta_{\mu\nu}. \tag{2.8}$$

Taking derivatives of (2.8), permuting the indices and making linear combinations of the differential equations derived in such a way, after some analysis we finally conclude that

$$\zeta^{\mu} = a^{\mu} + b^{\mu\nu}x_{\nu} + c^{\mu\nu\rho}x_{\nu}x_{\rho}, \tag{2.9}$$

where $b^{\mu\nu} = \alpha\,\eta^{\mu\nu} + \omega^{\mu\nu}$, for some $\alpha \in \mathbb{R}$ and $\omega^{\mu\nu}$ being antisymmetric, and $c^{\mu\nu\rho} = 2\eta^{\mu(\rho}b^{\nu)} - \eta^{\nu\rho}b^{\mu}$ for some vector b [26].

[2] Loosely speaking, it is the radius of curvature.

The transformation does not depend on a particular choice of coordinates, so we may consider every term in (2.9) separately. We immediately recognize that a^μ and $\omega^{\mu\nu}$ are the parameters of the Poincaré group; on the other hand, α is the parameter of the scaling transformation $x \to x' = e^\alpha x$, called *dilatation*, while the vector b determines what is known as the *special conformal transformation*: $x \to x' = \frac{x - x^2 b}{1 - 2b\cdot x + b^2 x^2}$. Thus we get the conformal group $\mathrm{SO}(2, d+1)$ as an extension of the Poincaré group [26].

It is expected that relativistic Poincaré-invariant theories are invariant under the whole conformal group at sufficiently high energies, but it is not the only application of CFT. Second-order phase transitions are characterized by the divergence of the correlation length, so that the system under consideration becomes scale invariant. In other words, the renormalization group flow ends at a stable fixed point and we loose the sense of scale. Therefore, we find that CFTs are equally well suited for condensed matter physics.[3] The same applies to quantum critical points, and experimental results imply that we should also consider conformally invariant quantum critical phases [15].

2.1.3 The large N limit

Not only that CFTs may be related to AdS space, but their supersymmetric versions also naturally arise in string theory, describing the systems with a large number of constituents. Before we close the circle matching such theories with general relativity in AdS spacetimes, we introduce an indispensable tool for managing the QFTs with many degrees of freedom. In our derivations we follow mainly [27].

Let us consider a Yang-Mills theory with N colors. It is a non-Abelian field theory, meaning that the gauge fields are represented by matrices in the adjoint representation of the $\mathrm{SU}(N)$ group. Its action (without matter) is given by

$$S_{YM} = -\frac{1}{2g^2}\int \mathrm{d}^4x\, \mathrm{Tr} F^2. \tag{2.10}$$

Let us redefine the coupling constant to be

$$\lambda = g^2 N. \tag{2.11}$$

This is the *'t Hooft coupling*, which is supposed to be fixed for every value of N [28]. The action then becomes

$$S_{YM} = -\frac{N}{2\lambda}\int \mathrm{d}^4x\, \mathrm{Tr} F^2. \tag{2.12}$$

The propagator is

$$\langle A^i_{\mu\, j}(x) A^k_{\nu\, l}(y)\rangle = \Delta_{\mu\nu}(x-y)\left(\delta^i_l\delta^k_j - \frac{1}{N}\delta^i_j\delta^k_l\right), \tag{2.13}$$

where $\Delta_{\mu\nu}$ is the propagator for a single gauge field, and the $1/N$ term arises because the $\mathrm{SU}(N)$ generators are traceless. In the large N limit the formula (2.13) reduces to

$$\langle A^i_{\mu\, j}(x) A^k_{\nu\, l}(y)\rangle = \Delta_{\mu\nu}(x-y)\delta^i_l\delta^k_j, \tag{2.14}$$

[3] An important difference is that such a scale invariance can be studied independently for time and space dimensions, when the time and space scalings are related by dynamical critical exponent. We will examine this in more detail in section 3.2.

while the symmetry group becomes effectively U(N).

The fact that the gauge fields are matrices is very convenient, because we can track the charge carried by each index separately. We can thus define new Feynman rules replacing the usual wavy line with two straight lines representing top and bottom indices. When such a line is closed, meaning that we have taken the trace, we get an additional factor of N. Following the standard rules for extracting the propagators and vertices from the action, we conclude that the propagator scales as λ/N, while the vertices scale as N/λ. Taking into account the new Feynman rules too, we see that an arbitrary Feynman diagram D scales as

$$D \sim N^{F+V-E}\lambda^{E-V}, \tag{2.15}$$

where F stands for the number of index loops (faces), E for the number of propagators (edges) and V for the number of vertices.

Further investigation of diagrams tells us that every diagram can be drawn on some Riemann surface, so we come up to the conclusion that diagrams can be equivalently described by the corresponding surface topology. Recalling the definition of the Euler characteristic $\chi = F + V - E = 2 - 2H$, we realize that a diagram scales according to the number of holes H of the Riemann surface:

$$D \sim N^{\chi}\lambda^{E-V}. \tag{2.16}$$

The important consequence is that in the large N limit planar diagrams (those that can be drawn on the sphere) are the leading ones, while all other diagrams are suppressed by a factor of $1/N$. Thus, provided that perturbation theory can be applied, summing only the planar diagrams simplifies the calculation to a great extent. The same applies for matter fields in the adjoint representation, except that the fields may need to be renormalized, so we can get N/λ in front of the action [27, 24, 15, 28].

We will be mainly interested in gauge-invariant operators that cannot be further decomposed, i.e. single-trace operators $\mathcal{O} = \mathrm{Tr}(\Phi_1\Phi_2\ldots)$. Adding source terms of the form

$$N\int \mathrm{d}^4x\, \mathcal{O}_i J_i \tag{2.17}$$

into the action, we are able to compute connected Green's functions by taking the functional derivatives of the generating functional $Z[\{J_i\}]$ with respect to the sources $\{J_i\}$:

$$\langle \mathcal{O}_1 \ldots \mathcal{O}_n\rangle_c = \frac{1}{(iN)^n}\frac{\delta^n \log Z[\{J_i\}]}{\delta J_1 \ldots \delta J_n}\bigg|_{J_i=0}. \tag{2.18}$$

We easily find that the n-point Green's function scales as N^{2-n}, which means that the connected part of a disconnected Green's function is subleading. Therefore

$$\langle \mathcal{O}_1 \ldots \mathcal{O}_n\rangle \approx \langle \mathcal{O}_1\rangle \ldots \langle \mathcal{O}_n\rangle, \tag{2.19}$$

and we may interpret the large N limit as a semiclassical limit (in the sense that long-range quantum correlations disappear and the correlation functions factorize). Such a factorization is an important property of the large N limit since it leads to decoupling and, consequently, complete suppression of multi-trace operators. That is the reason why we consider only the single traces [15].

2.2 AdS/CFT: the correspondence

The AdS/CFT correspondence relates a gravitational theory in the bulk of AdS_{d+2} spacetime with a $(d+1)$-dimensional CFT living on its boundary, with one theory being weakly and the other strongly coupled. The very idea that the bulk information is somehow encoded in its boundary gave birth to the synonym "holographic principle". The correspondence was proposed by Maldacena in 1997 [16] and fully established by Gubser, Klebanov, Polyakov and Witten in 1998 [17, 18] as a consequence of the duality between the open and closed strings in Type IIB string theory. In this section we will first briefly outline the original idea, motivation and theoretical background of AdS/CFT from string theory perspective. We will follow mainly the concept of [19]. Then, we will offer an alternative viewpoint, independent of string theory and based solely on CFT and general relativity (GR), which informally identifies the extra dimension of AdS with the energy scale of the renormalization group (RG) flow [15, 19].

String theory describes elementary particles as emergent entities – excitations of tiny vibrating one-dimensional objects. These are the open and closed strings. The way in which a string vibrates, its vibration frequency and tension, determine mass, charge and spin of a particle. Yet, strings are not the only objects string theory deals with. The ends of a string must satisfy some boundary conditions (for example, a closed string has periodic boundary conditions). Thus, if one end is fixed, we reveal a manifold defining the Dirichlet boundary condition. Such a manifold is a classical field configuration arising from closed strings. Depending on its dimension, we call it Dp brane, which is short for *p-dimensional Dirichlet membrane*. Therefore, a D0 brane is a point particle, a D1 brane is a string, while a D2 brane is a membrane. We will examine the behavior of D3 branes, three-dimensional generalizations of a membrane.

We consider a stack of N coincident D3 branes living in nine spatial dimensions (in the framework of IIB string theory). These branes gravitate and their gravitational strength depends on the string constant g_s. We will define

$$\lambda = g_s N. \tag{2.20}$$

If $\lambda \ll 1$, gravitational effects are negligible and we get N coincident D3 branes living in flat space. Such a system has low-energy excitations carried by N^2 strings stretched between all possible pairs of branes. The symmetries under the permutations of starting and ending branes form the $\mathrm{SU}(N)$ group. This symmetry and other general requirements lead to the conclusion that the open string excitations define an $\mathcal{N}=4$ super Yang-Mills (SYM) theory. It is a conformal quantum field theory with the Lagrangian density given by

$$\mathcal{L} \propto \frac{N}{\lambda}\mathrm{Tr}\left(F^2 + (\nabla\Phi)^2 + i\bar{\Psi}D_\mu\gamma^\mu\Psi + i\bar{\Psi}[\Phi,\,\Psi] - [\Phi,\,\Phi]^2\right). \tag{2.21}$$

This Lagrangian indeed has the $\mathrm{SU}(N)$ symmetry and all fields[4] in (2.21) are in the adjoint representation. It is easy to recognize λ as the 't Hooft coupling, with $g_s = g_{YM}^2$, and to conclude that in the large N limit we get the theory elaborated on in the previous section. We should also mention here that an open string stretching between two branes may be viewed as a closed string traveling from one brane to the other, thus revealing the *open-closed string duality*.

[4]Besides N^2-1 gauge fields, there are six bosonic fields Φ and four fermionic fields Ψ.

Now, let us consider the opposite limit, $\lambda \gg 1$. In this case the gravity is strong and the branes collapse upon themselves. As a result we get an object called *black brane*. Its name suggests similarity with a black hole; and indeed, it can be described by a planar black hole solution of the Einstein equations. Accordingly, a black brane has an event horizon, which is the place of infinite redshift, as measured by an observer at infinity. Therefore, the low-energy excitations in this case occur in the vicinity of the horizon, while their carriers are now closed strings.

Expanding the black brane solution in the vicinity of the horizon, we find[5] that the near-horizon geometry looks like $AdS_5 \times S^5$. Its metric is

$$ds^2 = \frac{L^2}{z^2}\left(-dt^2 + dz^2 + \sum_{i=1}^{3} dx_i^2 + z^2 d\Omega_5^2\right). \tag{2.22}$$

The t and x_i coordinates correspond to the brane worldvolume, while the five-sphere surrounds the brane at the radius $1/z$. Neglecting S^5, we see that the theory effectively lives in AdS_5 space-time with Minkowski boundary, as we noticed at the end of 2.1.1.

The AdS radius in (2.22) satisfies:

$$L = \lambda^{1/4} l_s = N^{1/4} l_P. \tag{2.23}$$

In the large N limit $L \gg l_s$ and $L \gg l_P$, so high energy excitations and quantum gravity effects governed respectively by l_s and l_P can be neglected. What remains is the classical theory of gravity, and the low energy spectrum of the black brane can be described by general relativity.

Following the already established open-closed string duality and the fact that both of these limits have SO(2, 4) symmetry, Maldacena came to the idea that these two descriptions could be matched too. He proposed that the system of N D3 branes in IIB string theory could be described either by IIB supergravity on $AdS_5 \times S^5$ or by $\mathcal{N} = 4$ SYM living on the AdS boundary. On top of that, if $\mathcal{N} = 4$ SYM is weakly coupled, gravity should be strongly coupled and vice versa. Therefore, as we have noticed in the previous paragraph, in the large N limit ($\lambda \gg 1$) we get a non-perturbative quantum field theory equivalent to classical gravity. The AdS/CFT correspondence thus indeed represents a weak-strong duality.[6] It is also a *holographic duality*, because the CFT living on the boundary of AdS space-time seems to act as a hologram with respect to the AdS bulk.

Soon after Maldacena's discovery other types of this correspondence were also found; and today, it is often applied independently of the string-theoretical framework. There are even conjectures that the holographic principle is a fundamental law of nature, independent of string theory or more fundamental than strings, but such ideas are still quite speculative. It is also believed that for $\Lambda > 0$ holography applies too, but dS/CFT is still poorly understood.

Although the duality is often labeled as a conjecture at the level of rigor of mathematics or mathematical physics, it is strongly supported by physical reasoning and numerous

[5] Since we start from the full ten-dimensional string theory, the black brane solution also lives in ten dimensions.

[6] This is the S-duality. It establishes a link between type I and heterotic-O, as well as type IIA and heterotic-E string theories. Under this mapping IIB string theory is *self-dual*, because both the CFT and the gravity sector belong to the same theory.

examples, so at the usual level of rigor in physics it is a well-established result. In the next section we will explain some practical aspects of holographic calculations.

However, before we proceed, we should present another, less formal, but more intuitive perspective on holography. Let us observe a $(d+1)$-dimensional CFT on different energy scales, i.e. the copies of the same theory along the renormalization group flow, from the IR to the UV limit. Let the energy scale be r. Considered as an additional dimension, it yields a curved $(d+2)$-dimensional space-time. If we want to preserve the conformal invariance, the form variation of its metric should vanish, meaning that the scaling transformation must be an isometry. That constrains the form of the "CFT+r" metric to be

$$ds^2 = f(r)\eta_{\mu\nu}dx^\mu dx^\nu + g(r)dr^2, \tag{2.24}$$

where the Greek indices denote the CFT coordinates. Taking into account that r is an energy scale, we know that under the transformation $x^\mu \to x'^\mu = \lambda x^\mu$ it should scale as $r \to r' = r/\lambda$. The metric then must be

$$ds^2 = \frac{r^2}{L^2}\eta_{\mu\nu}dx^\mu dx^\nu + \frac{L^2}{r^2}dr^2. \tag{2.25}$$

We recognize exactly an AdS space-time – if we define $z = 1/r$, the previous formula is identical to (2.6). The correspondence thus relates the RG flow with the dual theory of gravity, which is sometimes expressed as RG = GR [15].

This point of view is convenient and quite common in practice, but it may not be completely true. Its validity is still a research topic and calls for a revision.

Recalling that the vacuum state of a boundary CFT corresponds to pure AdS, one naturally expects that a modification of CFT (i.e. addition of new terms into the action) induces a modification of the gravity sector (which is considered equivalent to the change in the RG flow). Therefore, one needs to add new terms into the Einstein-Hilbert action [15, 24]. The choice of these terms will be discussed in the next section.

2.3 Holographic dictionary

Suppose that the AdS bulk contains a set of fields $\{\phi_i\}$. The presence of these fields modifies the metric, but, due to the cosmological constant, the space-time remains asymptotically AdS. We want to find the generating functional for such a system. Since the data at the AdS boundary determine the solution in the interior (together with some reasonable conditions for the deep interior), it makes sense to consider the action as a functional of boundary values of the bulk fields, which gives [15, 19, 24]

$$Z_{bulk}[\{\phi_i(x,z)|_{z=0} = h_i(x)\}] = \int \prod_i \mathcal{D}\phi_i \, e^{iN^2 S_{bulk}[\{\phi_i\}]}, \tag{2.26}$$

with $x = (t, \mathbf{x})^{\mathrm{T}}$. An important insight, made by Gubser, Klebanov, Polyakov and Witten in 1998 [17, 18], was that, due to the correspondence, a generating functional defined in this way equals the generating functional of the boundary theory, with the boundary values of the bulk fields taking the role of sources in the dual CFT [19], i.e.

$$Z_{bulk}[\{h_i(x)\}] = Z_{CFT}[\{h_i(x)\}]. \tag{2.27}$$

This is the famous *GKPW formula*, which enables us to do computations. More than that: this relation suggests that the AdS/CFT correspondence may be valid regardless of the string theory framework, relaxing its constraints to a few specific dualities. As a result, we are able to apply the so-called *bottom-up* approach where the basics of the correspondence can be understood just from the symmetries and perturbative dynamics of semiclassical gravity, allowing us to "engineer" the bulk and boundary theories according to our own needs. It stands in contrast to the *top-down* approach, when string theory constrains their content [15].

Still, (2.27) looks a bit complicated. Therefore we pass to the Euclidean coordinates. If the coupling on the gravity side is weak, meaning that the CFT on the boundary is strongly coupled, the partition function (2.26) can be approximated by its saddle point [24, 19]. We obtain

$$\left\langle e^{N\int \mathrm{d}^{d+1}x\,\mathcal{O}_i(x)h_i(x)}\right\rangle_{CFT} \approx e^{-N^2 S_{bulk}[\{\phi_i^*(x,z)|_{z=0}=h_i(x)\}]}. \tag{2.28}$$

Here $\{\phi_i^*\}$ are the solutions to the bulk equations of motion.

The factor of N^2 in front of the bulk action is singled out for convenience, because the leading terms of the effective action of the CFT in the large N limit are of the same order. From now on we drop it out, because it can be absorbed into the action.

Now we are able to compute Green's functions according to (2.18). We have to find the bulk action and take functional derivatives with respect to the boundary sources $\{h_i(x)\}$. But how does one relate the CFT operators to the operators in the bulk? The answer is provided by symmetry.

Let us consider a bulk gauge field A^a. It generates local symmetries in the bulk and couples to some current J^a. If we transform it as $A^a_\mu \to A^a_\mu + \nabla_\mu \chi^a$, the corresponding boundary term of the action transforms to

$$\int \mathrm{d}^{d+1}x\,\sqrt{-\gamma}(A^a_\mu J^\mu_a - \chi^a \nabla_\mu J^\mu_a). \tag{2.29}$$

Symmetry obviously requires that $\nabla_\mu J^\mu_a = 0$. Clearly, J^a is a conserved current; and, according to the Noether's theorem, it should determine also a conserved charge. We thus conclude that a local symmetry in the bulk translates to a global symmetry at the boundary, while the bulk gauge fields source conserved currents of the dual QFT[7] [19].

Furthermore, the boundary terms should be invariant under rotations. Taking into account that the generator of rotations is angular momentum, we see that the dual operators must have equal spins. Therefore, spin is the second criterion for matching up the operators. Accordingly, a scalar field in the bulk should be dual to a boundary operator such as, for example, $\mathrm{Tr}F^2$, $\mathrm{Tr}\Phi^2$ or $\mathrm{Tr}(\bar{\Psi}\Psi)$; similarly, fermions should be dual to the single-trace operators containing an odd number of fermion operators Ψ [15, 19].

For the end of this section we note that, because the metric as a gauge field represents the graviton, these criteria indicate a duality between the metric and momentum-energy tensor. Consequently, every change in $T^{\mu\nu}$ (i.e. in the QFT stress-energy tensor) induces a change in the bulk geometry. It is equivalent to the modification of the RG flow anticipated in the previous chapter. Thus, the idea of RG description is in this case justified [15].

[7] AdS/CFT is therefore considered to be also a *global-local duality*.

2.4 Temperature and charge density

Suppose that we have an electrically charged field theory at finite temperature. How do we introduce the temperature and electric flux in its AdS dual? Recall that the charge density on the boundary is dual to a scalar potential in the bulk. The idea is to have something like a reservoir for these quantities. Recalling Hawking's discovery that black holes emit thermal radiation, we realize that temperature can be introduced by placing a black hole into the interior of the AdS space-time. On the other hand, electric field may be constructed in two ways. We have to put the electric charge into the gravity sector, and it can be done either by inclusion of a charged black hole/brane or some charged matter outside its event horizon. So we get what are usually called *fractionalized* and *cohesive* charge densities, respectively [19, 15]. We will use only the first approach. Accordingly, we have to examine black hole thermodynamics in more detail.

Following a series of thought experiments, Bardeen, Carter and Hawking eventually recognized the black hole equivalents of thermodynamic laws [29, 30]. It was in 1973, a year before Hawking finally proved that black holes are indeed dissipative [31]. For a black hole with mass M, angular momentum J, charge Q and event horizon area A, spinning at angular velocity Ω and sourcing electrostatic potential Φ, these laws state that

0. $\kappa = const$ at horizon;
1. $\delta M = \frac{\kappa}{8\pi G}\,\delta A + \Omega\,\delta J + \Phi\,\delta Q$;
2. $\delta A \geq 0$;
3. it is impossible to approach $\kappa = 0$ through any physical process.

Consequently, the temperature and entropy are given by

$$T = \frac{\kappa}{2\pi}, \quad S = \frac{A}{4G} = \frac{A}{4l_P}. \tag{2.30}$$

Here κ is the surface gravity. It is the force an observer at infinity should apply in order to keep a unit mass near the horizon at rest. Although it formally defines the temperature, we will use the Euclidean gravity approach, due to Hawking and Gibbons, to compute the temperature in a simpler way [15, 32].

The laws of black hole thermodynamics open many profound questions. Answering these questions is still a hot research topic, and the ultimate explanation perhaps depends on advances in quantum gravity [29, 33]. We will not discuss this in any detail, because these issues are mainly irrelevant for this thesis. We just note that the entropy scales with surface instead of volume. From the viewpoint of classical thermodynamics, this is very unusual, but it perfectly matches our idea that the system under consideration lives on the boundary of space-time: the entropy of the AdS bulk with a black hole appropriately corresponds to the entropy of a QFT with one dimension less.

We now continue the discussion on temperature. We have just seen its relation to the event horizon. As we know, the event horizon is a hypersurface of no-return where the metric components g_{tt} and g^{rr} vanish. Besides, it is of particular importance to us since it defines all of the boundary conditions for bulk fields. Recalling that the boundary is asymptotically always AdS, we see that the CFT actually depends on the geometry of the bulk interior (i.e. the type of black hole in the center of the space-time). It is equivalent

to the notion that a change in temperature is reflected only in the IR physics, leaving the UV region untouched [19]. So, we are actually going to examine the near-horizon geometry of an arbitrary black hole.

Consider a generic, diagonal black hole solution in spherical coordinates after Wick rotation:[8]

$$ds^2 = g_{tt}(r)d\tau^2 + \frac{dr^2}{g^{rr}(r)} + f(r)d\Omega_d^2. \tag{2.31}$$

We first expand the metric (2.31) near the horizon r_h and then introduce a new variable $\rho = 2\sqrt{r - r_h}/\sqrt{(g^{rr})'(r_h)}$ in order to get

$$ds^2 \approx \frac{\rho^2}{4} g'_{tt}(r_h)\,(g^{rr})'(r_h)d\tau^2 + d\rho^2 + f(r_h)d\Omega_d^2. \tag{2.32}$$

Because $\rho = 0$ for $r = r_h$, the first term in the previous formula vanishes, which is equivalent to shrinking the τ coordinate to a point. Taking into account that horizon is not a special point, and therefore cannot be singular, we realize that τ and ρ correspond to polar coordinates. With redefinition $\tau = 2\varphi/\sqrt{g'_{tt}(r_h)\,(g^{rr})'(r_h)}$ it is easily seen that τ has period $4\pi/\sqrt{g'_{tt}(r_h)\,(g^{rr})'(r_h)}$. Now, recalling that Euclidean time is β-periodic ($\beta = T^{-1}$), we finally find the relation defining the temperature:

$$T = \frac{\sqrt{g'_{tt}(r_h)\,(g^{rr})'(r_h)}}{4\pi}. \tag{2.33}$$

In this way we have found also the temperature dependence of the boundary QFT.

[8] Wick rotation may be a bit troublesome, because it erases the track of causality; but we are interested only in stationary systems in thermodynamic equilibrium, so it should not bother us.

Chapter 3

A look at AdS/CMT

In this chapter we review an important aspect of holographic duality in condensed matter physics: the classification of holographic ground states in terms of their scaling properties. The purpose of this review is twofold. We first want to show how the general formalism works in practice, preparing the reader for our original setup. On the other hand, we simultaneously introduce a few simple results relevant for the rest of this work.

3.1 RN metal

3.1.1 The Reissner-Nordström black hole

We analyze the Reissner-Nordström (RN) solution to the Einstein-Maxwell (EM) equations with a negative cosmological constant in $d+2$ dimensions. We want to study a system at finite temperature and finite density, so we put a charged black hole into the center of the AdS_{d+2} space-time. The metric solving the Einstein equations is

$$ds^2 = \frac{r^2}{L^2}\left(-f(r)dt^2 + \sum_{i=1}^{d} dx_i^2\right) + \frac{L^2}{r^2}\frac{dr^2}{f(r)}, \tag{3.1}$$

with $f(r)$ being a *redshift function*

$$f(r) = 1 + \frac{Q^2}{r^{2d}} - \frac{M}{r^{d+1}}, \tag{3.2}$$

where Q and M are respectively the charge and mass of the black hole. The event horizon is determined by $f(r) = 0$, which gives a quadratic equation. Depending on the parameters M and Q, it might have

1. no solution, which means that we have a naked singularity;
2. one, *extremal*, solution r_*;
3. two solutions, $r_\pm$.

For now, we are interested neither in the naked singularity nor in the inner horizon, if it exists. For our needs, all physics starts at the outer horizon.

Yet, we are obliged to say a few words on the extremal solution. It may be shown that the mass and charge, in order to give a non-negative discriminant, satisfy the inequality [15]

$$M \geq \frac{2d}{d-1}\left(\frac{d+1}{d-1}\right)^{\frac{d+1}{2d}} Q^{\frac{d+1}{d}}. \tag{3.3}$$

This means that an extremal black hole cannot entirely evaporate through radiation. There is a limit upon which the black hole "freezes", conserving its electrostatic energy. Such a black hole has a single, finite horizon which leads to a nonzero ground state entropy of the black hole, as well as of the dual field theory. It certainly contradicts the third law of thermodynamics, but we need not pay much attention to it, because AdS-RN is pretty much a toy model. Nevertheless, its implications for AdS/CMT were profound on a conceptual level.[1]

Now, let us again consider the near-horizon geometry. Expanding the metric near its extremal horizon[2] and transforming the radial coordinate to $\zeta = L_2^2/(r - r_*)$, with $L_2 = L/\sqrt{d(d+1)}$, we find

$$ds^2 = \frac{L_2^2}{\zeta^2}(-dt^2 + d\zeta^2) + \frac{r_*^2}{L^2}\sum_{i=1}^{d} dx_i^2. \tag{3.4}$$

Obviously, the low-energy physics is governed by the $\mathrm{AdS}_2 \times \mathbb{R}^d$ geometry. It is peculiar because it has an anisotropic scaling symmetry. Namely, the space coordinates do not scale, meaning that the scale invariance exists only in time. This is recognized as a *quasi-local (temporal) quantum critical state* in the boundary QFT. This is an extremely important result because such a scaling was observed both in experiment and in DMFT simulations. Although all these examples are very different from the predictions of AdS-RN regarding the details, they show that holography at least gives correct qualitative predictions of new physics in strongly correlated materials. Interestingly, the RN strange metal, as we call this model, does not have any tunable parameters defining a quantum phase transition. Instead, we are dealing with a quantum critical phase [15, 19].

We conclude this section citing the solution to the Maxwell equations. As we have explained, A_μ couples to J^μ in the boundary QFT. Since we are interested only in the charge density, we set $\mathbf{A} = 0$. On the other hand, we know that particle density couples to chemical potential. Setting the elementary charge to be $e = 1$, one readily finds that $A_t = \mu$ at the boundary. Demanding also that A_t vanishes at the horizon, we get [15, 19]

$$A_t = \mu\left(1 - \left(\frac{r_+}{r}\right)^{d-1}\right), \tag{3.5}$$

where we have traded all constant terms for μ.[3]

3.1.2 Green's functions I

Before we continue with the examination of the $\mathrm{AdS}_2 \times \mathbb{R}^d$ geometry, we digress for a while in order to sketch a derivation of holographic Green's functions. For simplicity, we

[1] Actually, it is easy to show that the horizon can be squeezed to zero if we introduce a dynamical coupling for electromagnetic field [15]. It is the Einstein-Maxwell-dilaton model, which we elaborate on in the next section.

[2] Notice that $f'(r_*) = 0$ at $T = 0$ according to (2.33). It is said that $f(r)$ has a double zero at the horizon.

[3] In the case of the extremal horizon: $r_+ \equiv r_*$.

consider a free scalar field in pure AdS_{d+2}. Its equation of motion reads

$$\frac{1}{\sqrt{-g}}\partial_\mu\big(\sqrt{-g}g^{\mu\nu}\partial_\nu\phi\big) = m^2\phi. \tag{3.6}$$

We are not interested in its complete solution; instead, we seek only its expansion near the boundary. Assuming the ansatz $\phi(t,\mathbf{x},z) = (z/z_h)^\lambda\phi(t,\mathbf{x})$, with $z_h = 1/r_h$, after performing the Fourier transformation $\phi(t,\mathbf{x}) \to \phi(\omega,\mathbf{k})$ we get a linear combination of two branches as the general solution [15, 19, 34]:

$$\phi(\omega,\mathbf{k},z) = A(\omega,\mathbf{k})\left(\frac{z}{z_h}\right)^{\lambda_-} + \ldots + B(\omega,\mathbf{k})\left(\frac{z}{z_h}\right)^{\lambda_+} + \ldots, \tag{3.7}$$

with

$$\lambda_\pm = \frac{1}{2}\left(d+1 \pm \sqrt{\frac{(d+1)^2}{4} + m^2L^2}\right). \tag{3.8}$$

Demanding that $\lambda_\pm \in \mathbb{R}$, we constrain possible values of the mass-squared: $m^2L^2 > -(d+1)^2/4$.[4] This is the celebrated Breitenlohner-Friedmann (BF) bound, which has to be obeyed to avoid an instability of the AdS boundary [15].

The role of the two branches in (3.7) is determined by their exponents $\lambda_\pm$. Roughly speaking, the on-shell boundary action has the form

$$S_{bdy} \propto \oint_{z=\epsilon} \mathrm{d}\omega\,\mathrm{d}^d\mathbf{k}\left(2\lambda_- A^2 z^{-\sqrt{\frac{(d+1)^2}{4}+m^2L^2}} + (d+1)AB + \ldots\right), \tag{3.9}$$

where we have taken into account that the induced metric on the boundary and the outward pointing unit normal read $\gamma_{\mu\nu} = (L^2/\epsilon^2)\eta_{\mu\nu}$ and $n = -(\epsilon/L)\partial_z$, respectively. Since we suppose the limit $\epsilon \to 0$, the first term in (3.9) is potentially divergent and needs to be renormalized. Upon introduction of an appropriate counterterm, we are left with the first subleading term $\propto AB$, so we realize that A and B take the roles of the boundary source and current, respectively [15, 19].

Writing the leading power of (3.7) a bit differently, we can single out the dimension of the boundary space-time: $\lambda_- \equiv d+1-\Delta$,

$$\Delta = \frac{1}{2}\left(d+1+\sqrt{\frac{(d+1)^2}{4} + m^2L^2}\right). \tag{3.10}$$

Since the scalar field should remain invariant under the scaling transformation, meaning that the source scales as $A \to \lambda^{\Delta-d-1}A$, it is easy to conclude that Δ represents the scaling dimension of the dual operator [19]:

$$\mathcal{O}(x) \to \lambda^{-\Delta}\mathcal{O}(\lambda x). \tag{3.11}$$

Finally, we observe that, according to linear response theory, we could also have said that B is a response to the source A. Then the Kubo formula tells us that $B \propto A$, and we reveal the two-point correlation function:

$$G(\omega,\mathbf{k}) \propto \frac{B(\omega,\mathbf{k})}{A(\omega,\mathbf{k})}. \tag{3.12}$$

A specific contour choice for G (yielding e.g. a retarded propagator) is determined by the near-horizon boundary conditions. In order to obtain the exact relation, one should analyze the boundary action in detail [15, 34]. Since it is not of interest for us now, we leave it out.

[4] AdS space-times allow for the negative mass-squared fields.

3.1.3 Green's functions II

The above conclusion can be readily applied to the case of AdS_2 as the IR region of the AdS-RN space-time. The result is thus often called "IR Green's function" [35, 19]:

$$G_R^{(IR)}(\omega, \mathbf{k}) \propto \omega^{2\nu_k}, \tag{3.13}$$

with

$$\nu_k = \sqrt{\frac{1}{4} + m^2 L_2^2 + \frac{e^2 L^2 k^2}{8\pi G(d-1)^2 \mu^2}}. \tag{3.14}$$

It is obtained from the boundary solution to the equation (3.6) in one space dimension and in the $\omega \to 0$ limit, with the metric given by (3.4) [19]

$$\phi_{IR}(\mathbf{k}, \zeta) \approx A_1 \zeta^{1/2-\nu_k} + A_2 \zeta^{1/2+\nu_k}. \tag{3.15}$$

Since ζ in (3.15) can be rescaled by ω [35], a generic form of Green's function (3.12) clearly yields the relation (3.13).

The exponent ν_k is dependent on momentum k, but otherwise the propagator is momentum-independent, which implies a large number of degrees of freedom at low energy [19]. This property stems from the anisotropic scaling described in 3.1.1.[5]

A difficulty arises when one wants to compute the full low-energy Green's function. Namely, it is impossible to take the limit $\omega \to 0$ and simplify the equation of motion because it involves a term of the form $\sim \omega^2 \zeta^2 \phi$ which diverges in the very-near-horizon limit ($\zeta \to \infty$). Hopefully, it can be shown that for $\omega \ll \mu$ there exists an overlapping region on the $\omega\zeta$ scale, where $\omega\zeta$ can be made arbitrarily small at the very horizon (due to the definition of ζ), so that (3.15) indeed holds at the IR boundary, coinciding at the same time with the solution in the remainder of the bulk [19, 35].

This "full" bulk solution reduces to the form of (3.7) at the full AdS-RN boundary, i.e. in the $z \to 0$ limit:

$$\phi(\omega, \mathbf{k}, z) \approx B_1 z^{d+1-\Delta} + B_2 z^{\Delta}. \tag{3.16}$$

Since the scalar field is real, with a linear equation of motion, one can view the coefficients B_i as linear combinations of A_i ($i = 1, 2$). The resulting full Green's function is then

$$G_R(\omega, \mathbf{k}) = \frac{b_{21} + b_{22}\, G_R^{(IR)}}{b_{11} + b_{12}\, G_R^{(IR)}}, \tag{3.17}$$

where the coefficients b_{ij} are, in principle, functions of ω and $\mathbf{k}$. This is the well-known *matching procedure*, often used in AdS/CMT [19, 35]. We see that the low-frequency scaling of the spectra depends exclusively on the IR geometry [19].

A similar analysis applies to the fermions; only the exponents ν_k and the coefficients b_{ij} differ.[6] What is interesting in this case is the possibility to expand the Green's function around the Fermi surface (i.e. to expand the coefficients b_{ij} around $\omega = 0$). Since it is determined by the zero of the denominator in (3.17), the necessary condition for its existence is that $b_{11}(0, \mathbf{k}_F)$ vanishes. Then the Green's function takes a familiar form [15, 19]:

$$G_R(\omega, k_\perp) \approx \frac{Z}{\omega - v_F k_\perp - \mathrm{Im}\Sigma(\omega, k)}, \qquad k_\perp \equiv k - k_F. \tag{3.18}$$

[5] It corresponds to the limit $\mathbf{z} \to \infty$ of the Lifshitz scaling, as we are going to show in the next section.

[6] A generic fermionic Green's function is a matrix and so are the coefficients b_{ij}. Specifically, in the case of the AdS-RN Green's function these quantities are complex numbers.

The imaginary part of the self-energy scales as $\mathrm{Im}\Sigma(\omega, k) \propto \omega^{2\nu_k}$. Since it determines the lifetime of excitations, three cases are naturally distinguished [15, 19, 35]:

1. if $2\nu_{k_F} > 1$, quasiparticles are well-defined and long-lived, but are not necessarily of Landau type, with the ω^2 scaling;

2. if $2\nu_{k_F} = 1$, the self-energy becomes $\Sigma(\omega) = \hat{\Sigma}\,\omega \log(\omega/\mu)$ (with $\hat{\Sigma} \in \mathbb{C}$), indicating the *marginal Fermi liquid*, sometimes used as a toy model of strange metals [3];

3. $2\nu_{k_F} < 1$, which gives a divergent decay-rate, so we loose every trace of quasiparticles, although the Fermi surface remains present.

The RN metal thus succeeds in describing the properties of Fermi surfaces with and without quasiparticles. Actually, it was the first holographic construction to demonstrate a rise of non-Fermi liquids in a controlled way. Yet, this model has to be improved in order to give us more flexibility and versatility when it comes to the realm of its application.

3.2 EMD theory and the scaling atlas

Einstein-Maxwell theory can be enhanced by addition of a scalar field Φ. We consider a particular theory which turns the gravitational and gauge couplings into the Φ-dependent functions. Such a field is called *dilaton* and arises naturally in string theory setups as an indispensable ingredient of top-down models. Exploring its origin is beyond the scope of this work. Instead, we take it as a phenomenological generalization of the model, allowing the coupling constants of gravity and electromagnetism to go dynamical. We follow [15] and [19] for the most part.

The Lagrangian now reads

$$\mathcal{L} = \frac{R - 2\Lambda}{16\pi G} - \frac{1}{2}(\partial\Phi)^2 - \frac{Z(\Phi)}{4}F^2 - V(\Phi). \tag{3.19}$$

In accordance with the usual practice, we have redefined the metric in order to preserve the Einstein-Hilbert action with a constant gravitational coupling (this is called *Einstein frame* as opposed to string frame).[7] The only dynamical coupling left is then $Z(\Phi) = e_{eff}^{-2}$.

Z and V may have different forms (with a common property that the choice of $\Phi = 0$ must restore the usual EM action); in string theory, these are typically linear combinations of exponentials, obtained from the requirement for conformal invariance on the worldsheet. Therefore, these functions depend at least on two free parameters, called respectively α and δ, resulting in a whole family of EMD theories at our disposal. All of them give rise to a decoupled IR geometry with a specific scaling, allowing us at the same time to approach the naked singularity. The most general form of a deep IR metric at zero temperature is then

$$ds^2 = \left(\frac{r}{R}\right)^{-2\theta/d}\left(\frac{-r^{2\mathbf{z}}dt^2 + r^2\sum_{i=1}^{d}dx_i^2}{L^2} + \frac{L^2}{r^2}dr^2\right), \tag{3.20}$$

where R is a constant of integration.

If $\theta = 0$, this is the *Lifshitz metric*. It is described by the *dynamical critical exponent* $\mathbf{z}$; if different from unity, $\mathbf{z}$ indicates a different scaling of time and space coordinates. We

[7] EMD theories allow for inclusion of more than one scalar field. When there are a set of scalars, this redefinition cannot be done.

have already met such a geometry in the previous section: with redefinition $\lambda \to \lambda^{1/\mathbf{z}}$ the scaling $\{t, \mathbf{x}\} \to \{\lambda^{\mathbf{z}} t, \lambda \mathbf{x}\}$ of AdS_2 can be translated into a Lifshitz scaling with critical exponent $\mathbf{z} = \infty$.

On the other hand, θ is the *hyperscaling-violation exponent*. When $\theta \neq 0$, the metric (3.20) transforms as $ds^2 \to \lambda^{2\theta/d} ds^2$, so that, although covariant, it is no longer invariant to rescaling of coordinates, as the line element gets multiplied by $\lambda^{2\theta/d}$. The meaning of θ can be understood recalling that the perturbation of induced metric on the boundary sources the stress-energy tensor of QFT:

$$R^{\theta} \int \mathrm{d}^{d+1}x \, (\delta_0 \gamma)_t{}^t \epsilon. \tag{3.21}$$

Since the induced metric is obtained by stripping off the overall factor of $r^{-2\theta/d}/L^2$ in front of the Minkowski part of (3.20), we are eventually left with a dimensionful constant R^{θ}. Therefore, under a scaling transformation[8] $\{t, \mathbf{x}, r\} \to \{\lambda^{\mathbf{z}} t, \lambda \mathbf{x}, r/\lambda\}$ the energy density operator acquires an anomalous dimension θ. In other words, it transforms as $\epsilon \to \lambda^{-\Delta} \epsilon$, with

$$\Delta = \mathbf{z} + d - \theta \equiv \Delta_{\epsilon} - \theta, \tag{3.22}$$

where Δ_{ϵ} is the usual scaling exponent, arising when hyperscaling is not violated. The hyperscaling violation thus lowers the effective dimension of the system as well as the scaling dimension of the free energy, implying a decrease in the number of degrees of freedom and thereby the presence of the long-range entanglement.

We should emphasize that θ does not arise in Kadanoff's classical theory of critical exponents. It is a strictly quantum phenomenon, which justifies the classification of strange metals as quantum matter.

Solving EMD equations near the horizon, it is eventually possible to express the above exponents via the parameters α and δ. One then explicitly sees how the choice of EMD model determines the IR geometry. Recalling the supposed equivalence between the IR limit and a strange-metallic behavior, we expect that these parameters determine the strange metals too. In other words, we hope that defining the two-parameter family of classical theories of gravity we simultaneously end up with a classification of strange metals, i.e. with their "scaling atlas".[9]

[8] Note that $(\delta_0 \gamma)_t{}^t$ does not transform because of two different types of indices.

[9] One class within such a family should then comprise metals described by AdS_2 in IR. It may be shown that entropy density scales as $s \sim T^{(d-\theta)/\mathbf{z}}$, putting on the upper limit for θ. Keeping ratio $\eta \equiv -\theta/\mathbf{z}$ fixed and positive, with $\mathbf{z} = \infty$, we are able to reproduce an RN metal without the residual ground state entropy.

Chapter 4

A holographic lattice in 2D

4.1 The setup

As we have advertised in chapter 1, our aim is to offer a description of a strongly correlated system with an ionic lattice background in terms of holographic duality. We are interested in a square lattice in thermodynamic equilibrium. Since it is a static, finite density system at finite temperature, it is understood that the holographic dual is AdS_4 equipped with a charged black hole. Also, since the lattice is planar, we are going to use planar coordinates on the Poincaré patch introduced in 2.1.1.

We follow a path similar to the one explained in the previous chapter, with a few important differences. First, we note that the periodicity of the lattice, i.e. $\mathbb{Z}_4$ symmetry, implies a periodic chemical potential, with a modulation $\delta\mu$ superimposed on its mean value μ_0. Defining the lattice constant to be $a = 2\pi$, it equals

$$\mu(x, y) = \mu_0 + \delta\mu \cos x \cos y. \tag{4.1}$$

As we know, the boundary value of a gauge field should be

$$A_t(x, y, z)|_{z=0} = \mu(x, y). \tag{4.2}$$

We have set $e = 1$. For simplicity, we also define $8\pi G = L = 1$, which gives $\Lambda = -3$, according to (2.3).

Besides, a generic strange metal likely has some generic values for the exponents $(\theta, \mathbf{z})$, in contrast to the AdS_2 metal, where the spatial dimensions decouple from time in the $\mathbf{z} \to \infty$ limit and the hyperscaling is not violated (hence $\theta = 0$). Therefore, we expect to have two freely tunable parameters α and δ, which means that we keep the whole EMD action. So, in addition to the gauge field $A = A_t\, \mathrm{d}t$, we include also a dilaton field Φ. The bulk action is then

$$S = \int \mathrm{d}^4x\sqrt{-g}\left(\frac{R}{2} - \Lambda - \frac{1}{2}\partial^\mu\Phi\,\partial_\mu\Phi - V(\Phi) - \frac{Z(\Phi)}{4}F^{\mu\nu}F_{\mu\nu}\right) + S_{bdy}. \tag{4.3}$$

The last term in (4.3) comprises boundary terms. Its purpose is to cancel out the divergences which arise when one calculates the total action while computing, for example, Green's functions (see 3.1.2). These terms do not change the equations of motion and, since we are not interested in EMD correlators, we will not pay attention to them any more.

The potentials Z and V, obtained from the top-down approach, read

$$Z(\Phi) = \frac{Z_0}{2}(1 + \cosh(2\alpha\Phi)), \quad V(\Phi) = V_0(1 - \cosh(2\delta\Phi)). \tag{4.4}$$

Note that for $\Phi = 0$ the potential V vanishes, while Z reduces to unity, restoring the original coupling constant – we notice that Z_0 can be absorbed into the definition of A, so we set $Z_0 = 1$. Finally, varying the action (4.3) leads to the following set of equations:

1. *Einstein equations*

$$G_{\mu\nu} + \Lambda g_{\mu\nu} - \frac{1}{2}\partial_\mu\Phi\,\partial_\nu\Phi + \frac{Z(\Phi)}{2}F_\mu{}^\rho F_{\rho\nu} - \frac{1}{2}g_{\mu\nu}\mathcal{L}_m = 0, \tag{4.5}$$

   with the matter Lagrangian $\mathcal{L}_m = -\frac{1}{2}\partial^\mu\Phi\,\partial_\mu\Phi - V(\Phi) - \frac{Z(\Phi)}{4}F^{\mu\nu}F_{\mu\nu}$;

2. *dilaton equation*

$$g^{\mu\nu}\nabla_\mu\nabla_\nu\Phi - \frac{dV(\Phi)}{d\Phi} - \frac{1}{4}\frac{dZ(\Phi)}{d\Phi}F^{\mu\nu}F_{\mu\nu} = 0, \tag{4.6}$$

3. *Maxwell equations*

$$\nabla_\mu(Z(\Phi)F^{\mu\nu}) = 0. \tag{4.7}$$

This is in principle a system of fifteen nonlinear partial differential equations. Yet, diffeomorfism invariance of general relativity allows us to fix four components of the metric. We choose $g_{tx} = g_{ty} = g_{tz} = g_{xy} = 0$ in order to keep the time decoupled from space coordinates and to preserve the $\mathbb{Z}_4$ symmetry of the lattice. This symmetry then implies that we must have $g_{xx} = g_{yy}$ and $g_{xz} = g_{yz}$. Since the electric current density $\mathbf{J} = 0$, we conclude that the number of equations reduces to six.

We presented the equations in a compact form, because writing them out in full is very cumbersome and does not give any meaningful insight. Obviously, such a system cannot be solved analytically. We must perform a numerical integration, although even then finding the solutions gives rise to significant difficulties. We will discuss the numerics in the next chapter; but before that we thoroughly inspect the asymptotic behavior of the system.

4.2 IR geometry

4.2.1 The homogeneous solution

The homogeneous solution to the EMD equations is well known and can be found analytically for small r. The crucial simplification comes from the assumption that Φ is large near the extremal horizon ($r_h = 0$). Then the dilaton potentials (4.4) can be approximated by the exponentials:

$$Z = \frac{1}{4}e^{2|\alpha\Phi|}, \quad V = -\frac{V_0}{2}e^{2|\delta\Phi|}, \tag{4.8}$$

which stays in agreement with top-down results. These quantities are supposed to diverge, so constant terms in the action, including Λ, may be neglected. We follow the derivation presented in [36] by Iizuka et al.

The metric and electromagnetic field strength tensor are assumed to be respectively of the form

$$ds^2 = -a^2(r)dt^2 + \frac{dr^2}{a^2(r)} + b^2(r)(dx^2 + dy^2), \tag{4.9}$$

$$F = \frac{Q}{Z(\Phi)b^2(r)}\mathrm{d}t \wedge \mathrm{d}r; \tag{4.10}$$

where Q is a real constant. Plugging these ansätze into the EMD equations gives a simple, analytically solvable set of equations which fixes the form of a, b and Φ. Near the extremal horizon these functions are

$$a(r) = Cr^\gamma, \quad b(r) = r^\beta, \quad \Phi(r) = \kappa \log \frac{r}{R}, \tag{4.11}$$

with C and R being real constants. Such a constant is missing in $b(r)$ because the form of the metric (4.9) allows it to be absorbed in the definition of x and y. On the other hand, R may actually be neglected near the horizon, because $\log R$ is assumed to be a subleading term. We will therefore omit R in Φ for now. Note that $\gamma > 0$ is a necessary condition for $a(r)$ to be a redshift function.

Using the ansatz (4.11) and equating the powers and the coefficients of the leading terms in the equations of motion (4.5–4.7) one eventually finds the remaining parameters:[1]

$$\beta = \frac{(\alpha+\delta)^2}{1+(\alpha+\delta)^2}, \quad \gamma = 1 - \frac{2\delta(\alpha+\delta)}{1+(\alpha+\delta)^2}, \quad \kappa = -\frac{2(\alpha+\delta)}{1+(\alpha+\delta)^2}; \tag{4.12}$$

$$Q^2 = \frac{V_0(1-2\delta(\alpha+\delta))}{4+8\alpha(\alpha+\delta)}, \quad C^2 = \frac{V_0(1+(\alpha+\delta)^2)^2}{(2+4\alpha(\alpha+\delta))(1+(3\alpha-\delta)(\alpha+\delta))}. \tag{4.13}$$

A further insight of Iizuka et al. [36] was that a redefinition of the metric components by introducing a new redshift function:

$$a^2(r) \to C^2 r^{2\gamma}\left(1 - \left(\frac{r_h}{r}\right)^{2\beta+2\gamma-1}\right) \tag{4.14}$$

also satisfies the equations, so that one may extend the analysis to a finite horizon, as long as it is not too large.[2] Consequently, it is possible to determine the temperature of the black hole using (2.33):

$$T = \frac{C^2(2\beta+2\gamma-1)}{4\pi} r_h^{2\gamma-1}. \tag{4.15}$$

The metric (4.9) easily reveals the scaling of the entropy density: $s \sim r^{2\beta}$, and the previous formula transcribes it into the T-dependence. Demanding that the specific heat of the boundary theory is positive, we come to the constraint $2\gamma - 1 > 0$. Taking into account that C^2, Q^2 and γ are also positive, we end up with constraints on α and δ. Their domain is given in Table 4.1 and Figure 4.1.

Finally, for every value of r_h the Maxwell equation has the solution

$$A_t(r) = \frac{4Q(1+(\alpha+\delta)^2)}{1-(3\alpha-\delta)(\alpha+\delta)} r^{\frac{1-(3\alpha-\delta)(\alpha+\delta)}{1+(\alpha+\delta)^2}}. \tag{4.16}$$

[1] Our relations differ slightly from those in [36] because we have chosen different normalization of the kinetic terms in $\mathcal{L}_m$.

[2] That is, the approximation (4.8) must still hold.

$\delta \leq -1/2$	$\alpha > \delta + \sqrt{4\delta^2 - 1}$
$-1/2 < \delta < 0$	$\alpha > (1 - 2\delta^2)/(2\delta)$
$\delta = 0$	$\alpha \in (-\infty, \infty)$
$0 < \delta \leq 1/2$	$\alpha < (1 - 2\delta^2)/(2\delta)$
$\delta > 1/2$	$\alpha < \delta - \sqrt{4\delta^2 - 1}$

Table 4.1: The domain of the EMD parameters (δ, α).

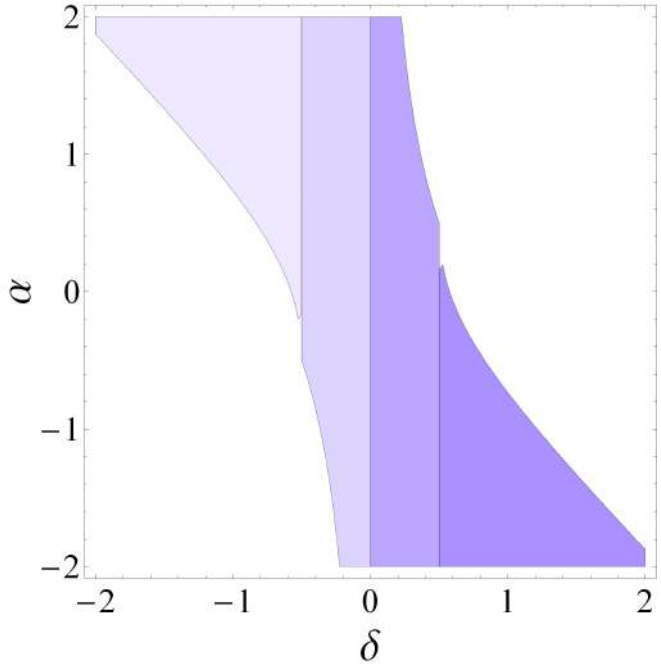

Figure 4.1: The domain of the EMD parameters (δ, α).

4.2.2 Lattice corrections

We have dedicated a great deal of time to investigate the homogeneous solution. It is because we expect that the anisotropy which stems from the $\mathbb{Z}_4$ symmetry only slightly perturbs the geometry near the horizon [21, 37], provided $\delta\mu/\mu_0 \leq 1$.[3,4] Therefore we use the previous solution as the leading term in a perturbative expansion

$$ds^2 = -a^2(r)S_{tt}(x,y,r)dt^2 + \frac{S_{rr}(x,y,r)}{a^2(r)}dr^2 + \\ + b^2(r)S_{xx}(x,y,r)(dx^2+dy^2) + 2(r-r_h)^{2\lambda}S_{xr}(x,y,r)(dx+dy)dr \quad (4.17)$$

[3]We suppose that greater amplitudes lead to more significant deviation from the homogeneous solution. We still have no idea what happens for $\delta\mu/\mu_0 > 1$.

[4]We thank A. Donos for discussions on this matter during the workshop "Strange metals: from the Hubbard model to AdS/CFT", which was held in May 2022 at the Institute of Physics Belgrade, Serbia.

with series corrections

$$S_{\mu\nu}(x,y,r) = \delta_{\mu\nu} + \sum_{n=1}^{\infty}(r-r_h)^n\Big(A_{\mu\nu}^{(n)} + B_{\mu\nu}^{(n)}\sin x\sin y + \\ + C_{\mu\nu}^{(n)}\sin x\cos y + D_{\mu\nu}^{(n)}\cos x\cos y + E_{\mu\nu}^{(n)}\cos x\sin y\Big). \quad (4.18)$$

Of course, $S_{xx} = S_{yy}$ and $S_{xr} = S_{yr}$ because of the lattice symmetry. The same reasoning applies to $A_t(x,y,r)$ and $\Phi(x,y,r)$.

Plugging in such expansions into the EMD equations with the approximate potentials (4.8), under the assumption that (4.12) holds, we determine the remaining exponents demanding the leading terms to have equal powers. Then we group terms of the same order obtaining a system of equations with unknown coefficients from the expansions (4.18). We have found that up to the second order all corrections are zero, meaning that the asymptotic IR solution to our equations is well approximated by the homogeneous one. Therefore, we are not going to include any of the IR corrections in further calculations.

This conclusion actually fits into the known result that explicitly (non-spontaneously) generated lattices are always irrelevant in deep IR at low temperatures [21]. The question in that regard, before we declare finding a homogeneous solution, is which T is sufficiently small and how much is "deep IR" really deep. Indeed, assuming $\delta\mu/\mu_0 \leq 1$, we intuitively expect the influence of the lattice on the IR physics to be weak; also, r_h (and therefore T) has to be small if (4.8) is expected to hold. Thus, we convince ourselves that our approximation fulfills the above conditions and is therefore justified.

4.2.3 Modification of the solution at finite horizons

We will now examine what happens if we move significantly away from the extremal horizon. Obviously, (4.8) ceases to hold and we must restore the full form of the potentials (4.4). We assume that the IR geometry remains mainly the same, with the ansatz (4.11) and finite-temperature correction (4.14). Yet, this time we do not neglect R.

The Maxwell equation is again satisfied by (4.10), but the dilaton equation at the lowest order in $(r-r_h)$ expansion now reads

$$4(\alpha+\delta)r_h^{\frac{4\alpha(\alpha+\delta)}{1+(\alpha+\delta)^2}} + 8\delta(1+2\alpha(\alpha+\delta))r_h^{\frac{4(\alpha+\delta)^2}{1+(\alpha+\delta)^2}}\sinh\frac{4\delta(\alpha+\delta)\log\frac{r_h}{R}}{1+(\alpha+\delta)^2} - \\ - \alpha(2\delta(\alpha+\delta)-1)\sec^2\frac{2\alpha(\alpha+\delta)\log\frac{r_h}{R}}{1+(\alpha+\delta)^2}\tanh\frac{2\alpha(\alpha+\delta)\log\frac{r_h}{R}}{1+(\alpha+\delta)^2} = 0. \quad (4.19)$$

A rough numerical analysis shows that the third term in (4.19) may be neglected, leading to an expression that can be easily solved analytically in R. The result is

$$R = r_h\exp\left(\frac{1+(\alpha+\delta)^2}{4\delta(\alpha+\delta)}\sinh^{-1}\frac{(\alpha+\delta)\,r_h^{-\frac{4\delta(\alpha+\delta)}{1+(\alpha+\delta)^2}}}{2\delta(1+2\alpha(\alpha+\delta))}\right). \quad (4.20)$$

Of course, one may find R numerically either; the results do not differ too much. What is particularly interesting, and very important, is that the relation (4.20) implies a vanishing dilaton in the limit of extremal horizon, since $R \approx r_h$ when r_h is small. However, it does

not contradict the result of subsection 4.2.1 because the initial neglecting of the term $\log R$ in (4.11) may be reinterpreted as its absorption into V_0 and Q.

Now, since F depends on Z, see (4.10), we have to re-integrate F_{tr} in order to find the modified solution for $A_t(r)$. Surprisingly, the solution can be found analytically; it reads

$$\begin{aligned} A_t(r) = -\frac{Q\, r^{1-2\beta}}{\alpha\kappa(1-2\beta+2\alpha\kappa)} \times \\ \times \left((1-2\beta+2\alpha\kappa)\, {}_2F_1\left(\frac{1-2\beta}{2\alpha\kappa}, 1, 1+\frac{1-2\beta}{2\alpha\kappa}, -\left(\frac{r}{R}\right)^{2\alpha\kappa}\right) - \right. \\ - \left(\frac{r}{R}\right)^{2\alpha\kappa} (1-2\beta)\, {}_2F_1\left(\frac{1-2\beta+2\alpha\kappa}{2\alpha\kappa}, 1, \frac{1-2\beta+4\alpha\kappa}{2\alpha\kappa}, -\left(\frac{r}{R}\right)^{2\alpha\kappa}\right) + \\ \left. + (1-2\beta+2\alpha\kappa) \tanh\left(\alpha\kappa \log\frac{r}{R}\right)\right), \end{aligned} \tag{4.21}$$

with β and κ given by (4.12). Here ${}_2F_1$ stands for hypergeometric function.[5]

Finally, when we put the ansätze into the Einstein equations, we find that the tt and rr components vanish in the $r \to r_h$ limit, while the xx component cannot be exactly satisfied. Nevertheless, numerical analysis shows that this deviation is small. We thus conclude that the homogeneous solution to the EMD equations can be maintained as the lowest-order approximation for an arbitrary r_h, though with minor modifications with respect to the low-temperature limit.

4.2.4 Critical exponents

Having examined the near boundary geometry, we are finally able to determine the critical exponents introduced in Section 3.2. In order to do that, it is necessary to relate the metric (4.9) with the form given by (3.20). We thus rewrite (3.20) in a new notation, with $d = 2$:

$$ds^2 = \left(\frac{\zeta}{\zeta_0}\right)^{-\theta} \left(-\zeta^{2\mathbf{z}} dt^2 + \zeta^2(dx^2+dy^2) + \frac{d\zeta^2}{\zeta^2}\right). \tag{4.22}$$

Equating the terms of the two metrics corresponding to g_{rr} and $g_{\zeta\zeta}$ one readily finds the relation between r and ζ:

$$r = \left(-\frac{4\sqrt{V_0}\,\delta(\alpha+\delta)}{\theta\sqrt{(2+4\alpha(\alpha+\delta))(1+(3\alpha-\delta)(\alpha+\delta))}} \left(\frac{\zeta}{\zeta_0}\right)^{-\frac{\theta}{2}} \right)^{\frac{1+(\alpha+\delta)^2}{2\delta(\alpha+\delta)}}. \tag{4.23}$$

Substituting the above expression into (4.9), we get a system of equations for θ and $\mathbf{z}$ and the constant ζ_0. Here we list the solutions:

$$\theta = \frac{4}{1-\alpha/\delta}, \tag{4.24}$$

[5] It is the solution to the Euler's hypergeometric equation with singular points 0, 1 and ∞, defined as

$${}_2F_1(\tilde{a},\tilde{b};\tilde{c};z) = \sum_{n=0}^{\infty} \frac{(\tilde{a})_n (\tilde{b})_n}{(\tilde{c})_n} \frac{z^n}{n!}$$

for $z \in \mathbb{C}$ and $|z| < 1$, with $(\tilde{q})_n$ being rising Pochhammer symbols (rising factorials).

$$\mathbf{z} = \frac{1+(\alpha-3\delta)(\alpha+\delta)}{\alpha^2-\delta^2}, \tag{4.25}$$

$$\zeta_0 = \left(\frac{\sqrt{V_0}(\alpha^2-\delta^2)}{\sqrt{(2+4\alpha(\alpha+\delta))(1+(3\alpha-\delta)(\alpha+\delta))}}\right)^{\frac{\alpha+\delta}{2\delta}}. \tag{4.26}$$

Although we often define $\zeta_0 = 1$, it is interesting to see explicitly how this quantity participates in coordinate transformations (aside from its role in counting the anomalous dimension of energy density).

However, in the context of a real experiment we expect to find θ and $\mathbf{z}$ from the measurement. Therefore, our task would actually be to determine α and δ, using the above-listed relations; and the obtained pair would then serve as an input data for numerical predictions. While the relations (4.24) and (4.25) generally cannot be inverted analytically, it is easy to perform a numerical fit to find (α, δ) from $(\theta, \mathbf{z})$.

4.3 UV asymptotics

In the preceding chapters we have learnt that the boundary value of the gauge field must be equal to the chemical potential, while the bulk geometry should be asymptotically AdS (which means that the metric must be analytic at infinity). Also, we have investigated the boundary behavior of a scalar field in pure AdS in subsection 3.1.2. Now we just generalize the results. For convenience, throughout this section we use the z coordinate instead of r; then the boundary lies, as we already know, at $z = 0$.

Under the assumption that the dilaton acquires a finite value near the boundary, we expand the potentials Z and V in Taylor series in order to slightly simplify the equations. We thus solve the simplified dilaton equation (4.6) in pure AdS_4 background, assuming it to be a good enough approximation. A generic solution should be sought again in the form of power series, meaning that the ansatz reads $\Phi(z) = (z/z_h)^\lambda$. In line with (3.7), it gives two branches:

$$\Phi(z) = \phi_1\left(\frac{z}{z_h}\right)^{3-\Delta} + \ldots + \phi_2\left(\frac{z}{z_h}\right)^{\Delta} + \ldots, \tag{4.27}$$

with

$$\Delta = \frac{3}{2}\left(1+\sqrt{1-\frac{16}{9}V_0\delta^2}\right). \tag{4.28}$$

Taking into account the BF bound, we reveal a new constraint: $V_0 < 9/(16\delta^2)$. A comparison with (3.8) then allows us to recognize the effective mass of the dilaton: $m_{eff}^2 = -4V_0\delta^2$. Since $3-\Delta > 0$, $\Phi(z)$ decreases towards the boundary (except for $\Delta = 3$). It means that we have obtained a consistent solution, proving the expansion of Z and V justified. We thus proceed with the inspection of the boundary limit of the metric.

We adopt similar ansätze as in subsection 4.2.2. The idea is to add subleading terms to the pure AdS_4 metric, so that it takes the form[6]

$$ds^2 = \frac{1}{z^2}\big(-S_{tt}(x,y,z)dt^2 + S_{xx}(x,y,z)(dx^2+dy^2) + \\ + 2S_{xz}(x,y,z)(dx+dy)dz + S_{zz}(x,y,z)dz^2\big), \tag{4.29}$$

[6]Recall that we have set $L = 1$.

where $S_{\mu\nu}(x, y, z) = \delta_{\mu\nu}$ to the leading order. Similarly, we restore the excluded terms of (4.27)[7] and modify the gauge field:[8]

$$A_t(x, y, z) = \mu(x, y) - \rho_{bulk}(x, y)\, z + \dots \quad . \tag{4.30}$$

Applying the same procedure as for the IR limit we have come to the conclusion that the equations of motion are satisfied again to first subleading order. We thus neglect the boundary corrections too.

[7] We take into account only the leading branch.

[8] It can be shown that the leading correction to A_t is the bulk charge density.

Chapter 5

The numerical solution

5.1 Numerical setup

The results obtained in the previous chapter give the insight into many important properties of the system, but are not particularly suited for numerical computations. Several tricks can help to gain a better control of the numerical integration. One is to introduce a new set of coordinates in order to compactify the space-time. A good choice is to replace r by a coordinate $\tilde{z}$ such that $\tilde{z} = 0$ at the horizon and $\tilde{z} = 1$ at the boundary.[1] This is realized by the transformation

$$\frac{r_h}{r} = 1 - \tilde{z}^2. \tag{5.1}$$

Next, it is convenient to rewrite the metric in a different form. The idea is to exploit the symmetry and to extract the factors that may diverge at some point, such as the redshift function and the pure AdS metric components (which are present at the boundary, where they also diverge). The remaining factors are then the unknown functions to be found. We denote them by $q_{\mu\nu}$. Thus, the ansatz for the metric reads

$$ds^2 = \frac{r_h^2}{(1-\tilde{z}^2)^2}\Big(- f(\tilde{z})q_{tt}(x,y,\tilde{z})dt^2 + q_{xx}(x,y,\tilde{z})(dx^2+dy^2) + \\ + 2q_{x\tilde{z}}(x,y,\tilde{z})(dx+dy)d\tilde{z} + \frac{4\tilde{z}^2}{r_h^2 f(\tilde{z})}q_{\tilde{z}\tilde{z}}(x,y,\tilde{z})d\tilde{z}^2\Big), \tag{5.2}$$

with

$$f(\tilde{z}) = 1 - (1-\tilde{z}^2)^{\frac{1+(3\alpha-\delta)(\alpha+\delta)}{1+(\alpha+\delta)^2}}. \tag{5.3}$$

Similarly, since the dilaton has a branch cut at the boundary, we rewrite it in the following form:

$$\Phi(x,y,\tilde{z}) = (1-\tilde{z}^2)^{3-\Delta}\phi(x,y,\tilde{z}). \tag{5.4}$$

The unknown function $\phi(x,y,\tilde{z})$ is actually a correction to the leading boundary solution (4.27), with $\phi_1 \equiv 1$. Since $A_t(x,y,\tilde{z})$ has no singular or branch-cut terms to be factored out, we end up with six unknown functions: A_t, ϕ, q_{tt}, q_{xx}, $q_{\tilde{z}\tilde{z}}$ and $q_{x\tilde{z}}$.

The boundary conditions (BCs) follow naturally: at the AdS boundary all of $q_{\mu\nu}$, along with ϕ, obviously have to be unity, while $A_t = \mu$, so all the BCs at $\tilde{z} = 1$ are of Dirichlet type. The periodicity of the lattice leads to periodic BCs for x and y. On the

[1] Note that this coordinate differs from z used in the previous chapters, which ranges from 0 at the boundary to ∞ in the deep interior of the space-time.

horizon, though, we must demand regularity, which means that all the components of the metric should have a vanishing first derivative. Consequently, the metric should satisfy Neumann BC at $\tilde{z} = 0$ (with periodicity in x and y), while the gauge field and dilaton are expected to obey Dirichlet conditions again. It is because the strange metals do not break any symmetry, and no-hair theorem holds in the case of the extremal horizon [38], implying $\lim_{r_h \to 0} A_t(x, y, r_h) = \lim_{r_h \to 0} \Phi(x, y, r_h) = 0$. Since the matter fields have to change smoothly with increase in temperature, Dirichlet boundary conditions apply to the finite horizons too.

Finally, let us notice that the Einstein equations are not elliptic. If one uses an iterative method for solving the equations, as we do, this turns out to be potentially an obstacle, since the algorithm may not converge. In order to enforce the ellipticity and secure the convergence, one employs the *DeTurck trick*. It consists in identifying a *reference metric* $\bar{g}_{\mu\nu}$ with the same BCs as the metric one wants to find and constructing the one-form

$$\xi_\mu = \Gamma^\nu_{\mu\nu} - \bar{\Gamma}^\nu_{\mu\nu}, \tag{5.5}$$

where $\bar{\Gamma}^\rho_{\mu\nu}$ are the Christoffel symbols obtained from $\bar{g}_{\mu\nu}$. The Einstein equations are then modified by a redefinition of the Ricci tensor:

$$R_{\mu\nu} \to R_{\mu\nu} + \nabla_{(\mu}\xi_{\nu)}. \tag{5.6}$$

The DeTurck term $\nabla_{(\mu}\xi_{\nu)}$ enhances the convergence of the algorithm and eventually disappears when the solution is found [39].

5.2 Approximate solutions

Solving the full set of EMD equations is a demanding task. It calls for both time and hardware resources, in addition to necessary programming skills. Since it is not indispensable for the physical goal of this thesis, we do not pursue it here. Instead, we choose to solve the Maxwell and dilaton equations with an approximate metric solution as a background. The matter fields are thus treated in the probe limit. Such a solution is obviously not numerically exact, but is sufficient for our purposes. The solution to the full set of equations may be found in a somewhat different numerical setup in [20].

Since the above-considered boundary conditions must be satisfied also by the asymptotic solutions found in the previous chapter, a natural choice for an approximate solution is to sew them together. Were we to solve the full set of equations, such solutions would be the initial guesses, i.e. the first step of the iterative solution we are going to elaborate on in the next section. Since we are concerned only with the matter fields, this is true solely for A_t and ϕ. Nevertheless, we use the terms "approximate solutions" and "ansätze" interchangeably. Clearly, these functions are redefined by extracting the appropriate factors, as in (5.2) and (5.4). The subtlety is only that some factors need not be extracted from the asymptotic solution if they tend to unity for corresponding $\tilde{z}$. For example, the prefactor of (5.4) equals unity at the horizon, so it does not matter whether it is extracted or not.

Still, one has to be careful when sewing the solutions together. The asymptotics on both ends must be preserved and at the same time the resulting ansatz must be reasonably smooth everywhere. In that regard, we have defined the following function:

$$s_{m,n}(\tilde{z}) = (1 - \tilde{z}^m)^n, \tag{5.7}$$

for $m, n \in \mathbb{N}$ and $m \leq n$. It has the following properties:

1. $\lim_{\tilde{z}\to 0}(s_{m,n}(\tilde{z})u(\tilde{z}))^{(l)} = u^{(l)}(0)$
2. $\lim_{\tilde{z}\to 1}\left((1 - s_{m,n}(\tilde{z}))u(\tilde{z})\right)^{(l)} = u^{(l)}(1)$
3. $\lim_{\tilde{z}\to 1}(s_{m,n}(\tilde{z})u(\tilde{z}))^{(l)} = 0$

for an arbitrary smooth function $u(\tilde{z})$ and $l < m$. Obviously, we may use $s_{m,n}(\tilde{z})$ to continuously switch off the IR solution towards the boundary, while simultaneously switching the UV solution on, and vice versa. Still, the transition might be insufficiently smooth, giving unnatural peaks and bumps, especially inconvenient for the numerics; and here the exponent n comes into play. By changing n it is possible to fine-tune the approximate solution and transform it into a desired shape adjusting its smoothness at will. The only constraint is that we must take $m \geq 3$ if we are to preserve the first and second derivatives at the boundaries. The specific choices we have used for our system are listed bellow.

$$q_{tt}(x, y, \tilde{z}) = -s_{3,6}(\tilde{z})\frac{(1-\tilde{z}^2)^2}{r_h^2 f(\tilde{z})}g_{tt}^{(IR)}(\tilde{z}) + 1 - s_{3,3}(\tilde{z}) \tag{5.8}$$

$$q_{xx}(x, y, \tilde{z}) = s_{3,3}(\tilde{z})\frac{(1-\tilde{z}^2)^2}{r_h^2}g_{xx}^{(IR)}(\tilde{z}) + 1 - s_{3,3}(\tilde{z}) \tag{5.9}$$

$$q_{\tilde{z}\tilde{z}}(x, y, \tilde{z}) = s_{3,3}(\tilde{z})\frac{(1-\tilde{z}^2)^2 f(\tilde{z})}{4\tilde{z}^2}g_{rr}^{(IR)}(\tilde{z}) + 1 - s_{3,6}(\tilde{z}) \tag{5.10}$$

$$q_{x\tilde{z}}(x, y, \tilde{z}) = \frac{(1-\tilde{z}^2)^2}{r_h^2}\tilde{z}^3 s_{3,3}(\tilde{z}) \tag{5.11}$$

$$A_t(x, y, \tilde{z}) = s_{3,3}(\tilde{z})A_t^{(IR)}(\tilde{z}) + \tilde{z}^2\mu(x, y)(1 - s_{3,3}(\tilde{z})) \tag{5.12}$$

$$\phi(x, y, \tilde{z}) = s_{3,6}(\tilde{z})\Phi^{(IR)}(\tilde{z}) + 1 - s_{3,3}(\tilde{z}) \tag{5.13}$$

By $g_{\mu\nu}^{(IR)}(\tilde{z})$ we have denoted the components of the near-horizon metric (4.9) after the coordinate transformation (5.1), while $A_t^{(IR)}(\tilde{z})$ and $\Phi^{(IR)}(\tilde{z})$ are obtained in a similar manner from (4.21) and (4.11), respectively. The UV part of $A_t(x, y, \tilde{z})$ is adapted from the solution of the EM equations (3.5).

As a natural quality test of the approximate solutions, we have evaluated the EMD equations on the functions (5.8–5.13). We have found that the equations hold almost identically, with the exception of a central region around the point $\tilde{z} \approx 0.6$, where the equations are strongly nonzero, resulting in a variety of peaks (two representative examples are given in Figure 5.1). Since the deviation from zero is rarely very large, we conclude that our guesses are of good enough quality, though.

Still, what is a bit peculiar is the sharpness of the peaks. We certainly expect that the equations are not satisfied in the region where the asymptotic solutions overlap, but we expect a wider and less steep deviation. Instead, we find that the IR solution is a very good approximation in almost one half of the domain. We have repeated this analysis for different ansätze (including the IR and UV solutions separately) and found the same behavior every time. It looks like the true solution is of domain-wall type, with a sharp transition from the large IR throat to the near-AdS UV region. Since this occurrence is not manifested in our results, we do not discuss it any more; instead, we turn us to the technical core of our research.

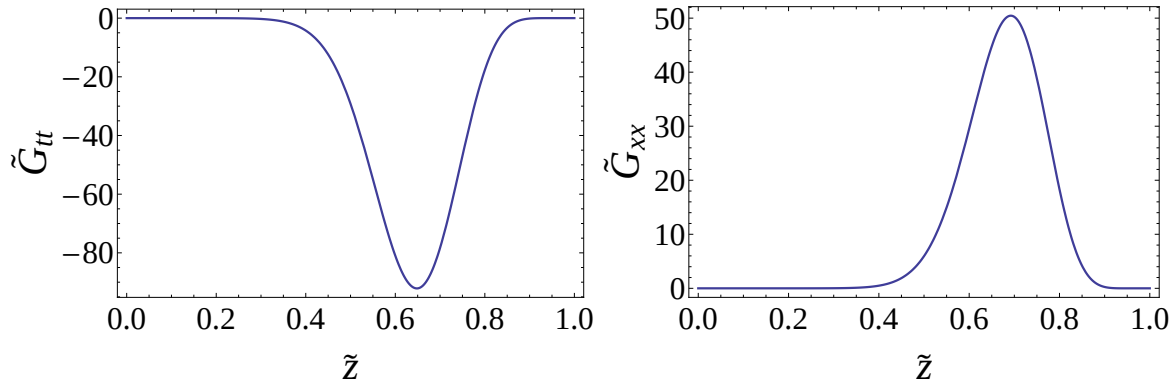

Figure 5.1: The tt and xx components of the Einstein equations along $\tilde{z}$, evaluated on the solutions (5.8–5.13) for $\mu_0 = 1$, $\delta\mu = 1$, $T = 0.5$, $V_0 = 0.5$, $\alpha = -1.5$ and $\delta = 1$ ($\tilde{G}_{\mu\nu} \equiv G_{\mu\nu} + \Lambda g_{\mu\nu} - \frac{1}{2}T_{\mu\nu}$). Since the profiles of the evaluated equations mostly do not depend on x and y, we have chosen the slice $x = y = 0$. Similar plots are obtained for the other equations.

5.3 Numerical methods

Current wisdom is that nonlinear systems of elliptic PDEs, such as our EMD equations, are best solved by the Newton-Raphson method, leading it to become the standard in applied holography [39, 40]. It could be used for solving either the whole system of equations or some subset thereof, or just a single equation. Here we give a brief description of the procedure, along with the consequent elaboration on differentiation methods. We follow mainly [40] and focus on a single equation since the generalization to the system is straightforward.

Consider a second-order nonlinear PDE

$$F[f''(x,y,z),\ f'(x,y,z),\ f(x,y,z),\ z] = 0 \tag{5.14}$$

with an approximate solution

$$f_1(x,y,z) = f(x,y,z) + h(x,y,z), \quad \|h\| \ll 1. \tag{5.15}$$

The idea is to find a better approximation f_2 and to repeat this procedure until for some $n_0 \in \mathbb{N}$ the variation h vanishes. We expect that for every $n < n_0$ the evaluation of F on f_n does not differ significantly from zero, so we expand F in the vicinity of the exact solution in order to obtain a linear equation in h:

$$F[f_n] = \sum_{i,j,k=0}^{2} \frac{\delta F[f_n]}{\delta f^{(i,j,k)}} h^{(i,j,k)}(x,y,z) + O(h^2), \tag{5.16}$$

where

$$f^{(i,j,k)}(x,y,z) \equiv \frac{\partial^{i+j+k} f}{\partial x^i \partial y^j \partial z^k}, \quad h^{(i,j,k)}(x,y,z) \equiv \frac{\partial^{i+j+k} h}{\partial x^i \partial y^j \partial z^k}. \tag{5.17}$$

Finding h, we are able to determine $f_{n+1} = f_n - h$, and so on. The convergence is reached when $\|h\| < \epsilon$ and $\|F[f_{n_0}]\| < \epsilon$ simultaneously, for some appropriately chosen norm and accuracy $\epsilon \in \mathbb{R}$.

Finding h in each iteration rests on discretizing the domain, transforming it into a $m \times n \times p$ grid:

$$D \subset \mathbb{R}^3 \to \tilde{D} = \{x_1, x_2, \ldots, x_m\} \times \{y_1, y_2, \ldots, y_n\} \times \{z_1, z_2, \ldots, z_p\}, \tag{5.18}$$

in order to replace f_n by an mnp-component vector[2]

$$\vec{f_n} = \big(f_n(x_1, y_1, z_1), \ldots, f_n(x_1, y_1, z_p), f_n(x_1, y_2, z_1), \ldots, f_n(x_m, y_n, z_p)\big)^{\mathrm{T}}. \tag{5.19}$$

Then all derivatives and all variations of the functional F become matrices and we end up solving a linear system of algebraic equations. Namely, $\delta F[f_n]/\delta f^{(i,j,k)}$ are evaluated at every point of $\tilde{D}$ in order to give the diagonal elements of the corresponding $mnp \times mnp$ matrices; we denote them by $C^{(i,j,k)}(\vec{f_n})$. Similarly, the evaluation of $F[f_n]$ on $\tilde{D}$ gives the "right-hand-side" vector $\vec{F}(\vec{f_n})$, so that the linearization (5.16) reads

$$\sum_{i,j,k=0}^{2} C^{(i,j,k)}(\vec{f_n}) D_{(i,j,k)} \vec{h} \equiv \mathbb{D}\,\vec{h} = \vec{F}(\vec{f_n}). \tag{5.20}$$

Here, the $mnp \times mnp$ matrices $D_{(i,j,k)}$ are, naturally, Kronecker products of the corresponding ordinary, "one-dimensional" differentiation matrices.[3] Inversion of (5.20) then leads to

$$\vec{h} = \mathbb{D}^{-1} \vec{F}(\vec{f_n}), \tag{5.21}$$

allowing us to compute $\vec{f}_{n+1}$, i.e. a better numerical approximation to the unknown function f.

Yet, this is actually an incomplete algorithm. In order to solve a differential equation we need to supplement it by boundary conditions; so the same applies to the matrices. Therefore, we have to delete the rows of $\mathbb{D}$ corresponding to the boundary points and replace them with appropriate boundary conditions [40, 41]. We do the same with $\vec{F}(\vec{f_n})$, with the notion that for h all BCs must be mapped to zero according to (5.15), since every approximation f_n has to obey the same BCs as f.

The accuracy of the above procedure depends on a couple of factors. First, we must choose a very good initial guess as an input for the first iteration, or the algorithm may not converge.[4] Second, the differential operator $\mathbb{D}$ may be near-singular and its inversion therefore may be difficult. This is especially the case if $\mathbb{D}$ is sparse, which leads us to the third observation. Namely, the solution to a great extent depends on the choice of differentiation method.

In order to avoid these caveats and additionally speed up the procedure, we have seized for the *pseudospectral collocation method*. Its essence lies in expanding a function in a series in whatever basis is convenient. For example, a 2π-periodic function f may be represented as a Fourier series:

$$f(x) = \sum_k c_k e^{ikx}. \tag{5.22}$$

[2] We use a different notation for numerical vectors. Unlike the Euclidean (geometric) vectors, denoted by bold letters, we represent them by letters accented by a right arrow.

[3] These matrices have dimensions $m \times m$, $n \times n$ and $p \times p$.

[4] The approximate solution for the initial guess must satisfy the same boundary conditions as the exact one and must resemble it as much as possible. On the other hand, it must not have any large gradients.

Its derivative at the i-th point of a homogeneous[5] m-point grid is then

$$f'(x_i) = \sum_k ikc_k e^{ikx_i}. \tag{5.23}$$

Expressing c_k via the inverse Fourier transform, one readily finds

$$f'(x_i) = \Delta x \sum_k \sum_j ike^{ik(x_i - x_j)} f(x_j), \qquad \Delta x = \frac{2\pi}{m-1}, \tag{5.24}$$

which means that the derivatives can be computed in a numerically exact way. Such a derivative operator can be represented as a matrix depending solely on the grid points x_j.

On the other hand, a non-periodic function $G(z)$, defined for $z \in [-1, 1]$, can be expanded as

$$G(z) = \sum_k a_k T_k(z), \tag{5.25}$$

with T_k being the Chebyshev polynomials. Upon setting $z = \cos x$, with $x \in [0, 2\pi]$ and x_i equally spaced (i.e. upon the identification of the points z_i with points on a circle), the Chebyshev polynomials can be represented as $T_k = \cos(kx)$, leading (5.25) to become a cosine Fourier series expansion of some symmetric function $g(x)$. Differentiation of G then gives

$$G'(z) = \frac{g'(x)}{\sqrt{1-z^2}}, \tag{5.26}$$

and we realize that the problem reduces to the previous case. One just needs to evaluate the function on the points defined above, known as the *Chebyshev grid*. The advantage of the pseudospectral method is thus in its speed (since it is based on a Fast Fourier Transform – FFT), and in the fact that the matrices obtained in such a way are dense, which decreases the possibility that they turn out singular.

5.4 The equation solver

We have performed all computations in `Wolfram Mathematica`, making use of the package `diffgeo.m` [42]. Additionally, FFT is implemented as a built-in function, and likewise the pseudospectral differentiation operators as an option to the `NDSolve` command. Representing these derivatives in matrix form is then straightforward.

Yet, an issue arises with the inversion of the differentiation matrix $\mathbb{D}$. We may simply solve the system of algebraic equations, using the command `LinearSolve`, or find the inverse of $\mathbb{D}$ and act on the right-hand-side of the equation. Since $\mathbb{D}$ may be ill-defined, or even singular (although it did not occur), seemingly the best option for inversion is the command `PseudoInverse`.

The pseudoinverse of a matrix A, A^+, is a generalization of the inverse which solves the system of equations approximately, finding the "best fit" by the method of least squares. It satisfies $AA^+A = A$ and $A^+AA^+ = A^+$, with AA^+ not necessarily being the identity matrix. The corresponding command in `Mathematica` thus deals extremely well with all possible matrix constructions, but has a significant drawback since it "oversees" the boundary conditions, leading to nonzero values at the places where one would expect

[5] A homogeneous grid has all points equally spaced.

the components to vanish. As a consequence, one gets the solutions satisfying wrong boundary conditions.

On the other hand, the inverse obtained by `LinearSolve` obeys BCs very well, but is prone to delivering significant errors if the coefficients in equations span a set of values that differ by a few orders of magnitude. Since the system we have chosen to solve gives relatively well-defined matrices (for a reasonable choice of parameters), we have used this command nevertheless.[6]

However, the code is still very sensitive to the input data. It means that we are still not able to find solutions for the full range of parameters, in addition to the already mentioned necessity of good ansätze. But this is to be expected for a system of multidimensional nonlinear equations. Some parameter regimes we exclude from the beginning: we do not expect to find solutions at very high or very low temperatures, or with strongly varying chemical potential.

5.5 The scalar and gauge field solutions

In this section we present the solutions for A_t and Φ. We recall that the free parameters are μ_0, $\delta\mu$, V_0, α, δ and T. We immediately set $T = 0.5$ since we are obliged to work at relatively low temperatures, according to the conclusions of subsection 4.2.2. Still, we do not take T too low for two reasons: first, we want to allow r_h to be arbitrarily large; second, in this way we avoid some possible numerical instabilities. Further, we set $V_0 = 0.5$ too, in order to satisfy the BF bound.

Now we have to choose α and δ. Our aim is to inspect different scaling geometries offered by the scaling atlas, and thereby different pairs (α, δ). Yet, practice shows that the choice $\Delta = 3$, leading to a non-vanishing dilaton at the boundary, enhances the stability of numerical integration to a great extent. Given $V_0 = 0.5$, such a conformal dimension is obviously obtained for $\delta = \pm 1$, so we choose to fix $\delta = 1$ and vary only α. It is sufficient to work in the domain of negative α ($\alpha < -0.732$ for $\delta = 1$ according to Table 4.1), because the choice of $\delta = -1$ ($\alpha > 0.732$), gives similar results – one only has to adjust the sign of the constant Q (see subsection 4.2.1) in order to maintain a positive gauge field.

Constraining the values of α and δ in such a narrow domain seems to contradict the purpose of this thesis, i.e. inspecting the parameter space for strange-metallic or Hubbard-like behavior, but is actually quite justified. Namely, it may be shown that the treatment of fermions in the probe limit in the homogeneous case gives the spectra which depend exclusively on the combination of the IR scaling exponents: $\beta+\gamma$ [20, 36]. In the presence of the lattice the situation is more complicated and the sum $\beta + \gamma$ is not the sole factor that determines the scaling of the spectral function, but it is still the most important one [20]. Since the spectra can be compared to experimental data, it suffices to vary only one of the EMD parameters in order to vary the sum $\beta + \gamma$.

Finally, we set $\mu_0 = 1$ and vary $\delta\mu$ measured in units of μ_0, since we are for now interested only in the ratio $\delta\mu/\mu_0$, not in $\delta\mu$ per se. We examine weak lattices, with $\delta\mu = 0.5$ and $\delta\mu = 1$, and also a moderately strong lattice, with $\delta\mu = 1.5$. For each of these values we take $\alpha = -1.5$ and $\alpha = -2$, obtaining two pairs of critical exponents: $(\theta, \mathbf{z}) = (1.6, 2.6)$ and $(\theta, \mathbf{z}) = (4/3, 2)$. The results are given in Figures 5.2–5.5. As a

[6] We have done many tests inspecting the efficiency of these commands. We had also taken into account the command `Inverse`, but we did not give much attention to it since the `PseudoInverse` equals the `Inverse` when a matrix is regular.

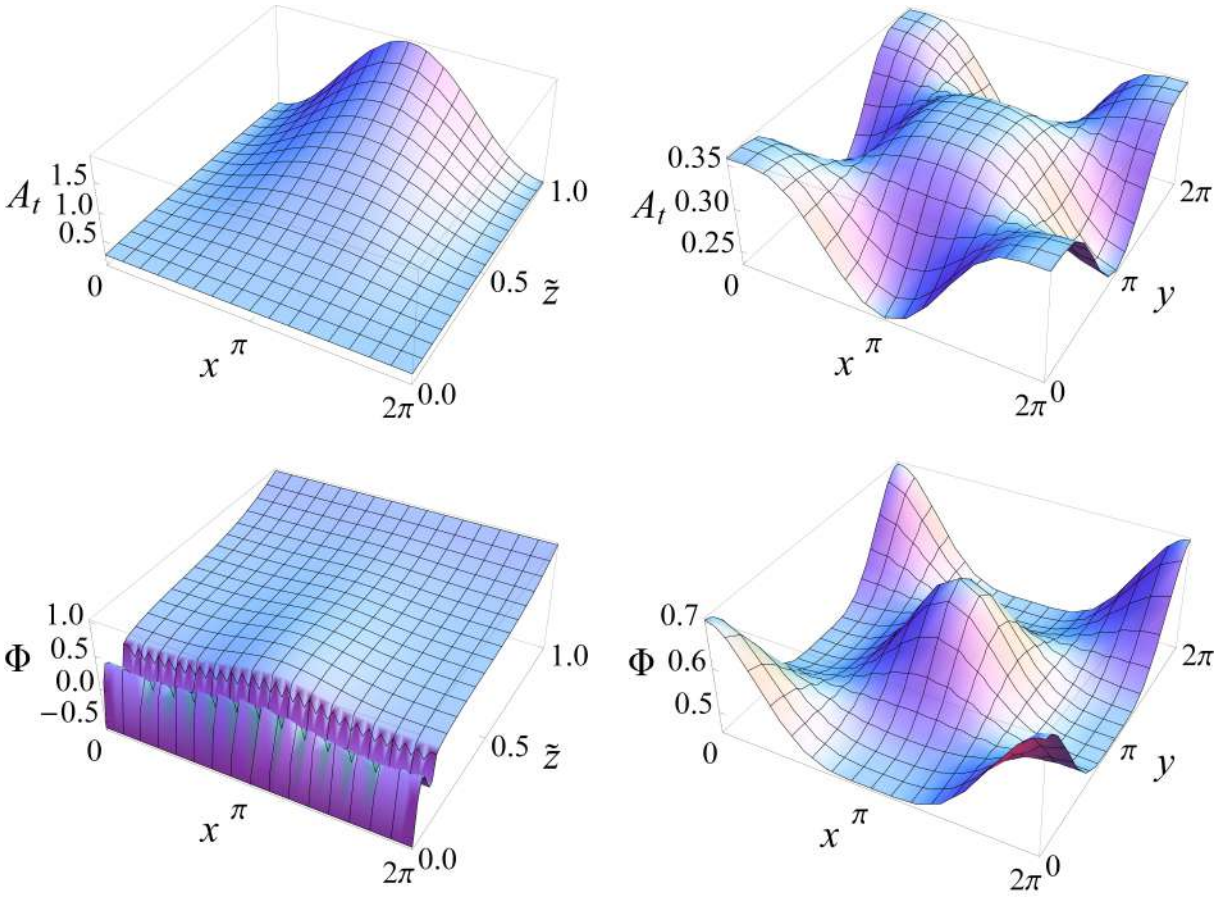

Figure 5.2: Numerically computed electrostatic (top) and dilaton (bottom) field along an x-$\tilde{z}$ slice at $y = 3.59$ (left) and along an x-y slice at $\tilde{z} = 0.22$ (right) for $\delta\mu = 1.0$ and $\alpha = -2.0$, with $\mu_0 = 1$, $\delta = 1$, $V_0 = 0.5$ and $T = 0.5$.

curiosity, we have also solved the system for $\mu_0 = 1$, $\delta\mu = 2$ and $\alpha = -1.5$, proving that our holographic setup may be applicable even in the presence of a strong lattice.

Actually, we have found a whole family of solutions for $\mu_0 \in \{0.5, 0.6, 0.7, \ldots, 1.5\}$ and $\alpha \in \{-2.3, -1.7, -1.5\}$, maintaining the ratio $\delta\mu/\mu_0 = 1$, in order to obtain the corresponding electric charge densities and examine how they depend on μ_0 and whether they change upon variation in α; but we postpone this discussion for the next chapter. In this section we are concerned solely with those properties of the solutions which depend on the relative strength of the lattice.

Figures 5.2–5.5 show that the strength of modulation determines the oscillatory behavior of A_t near the boundary, which is always damped towards the horizon, just as we expect. Yet, the overall profile of the field depends on α, i.e. on the IR solution. Accordingly, the value of A_t at the horizon can be either smaller or larger than its mean value at the boundary (μ_0), leading to totally different slopes along the $\tilde{z}$-axis. This is important because the charge density, discussed in the next chapter, depends on $\partial_{\tilde{z}} A_t$.

On the other hand, Φ generally maintains the same profile with respect to $\tilde{z}$, regardless of α.[7] Since we have fixed its value at $\tilde{z} = 1$, the influence of the lattice first increases towards the horizon, and then, very near the horizon, suddenly becomes negligible.[8] Such

[7] Notice that for $\Delta = 3$ we get $\Phi(x, y, \tilde{z}) = \phi(x, y, \tilde{z})$.

[8] The higher-frequency oscillations in the IR region, visible in x-$\tilde{z}$ plots, are most likely a subsidiary

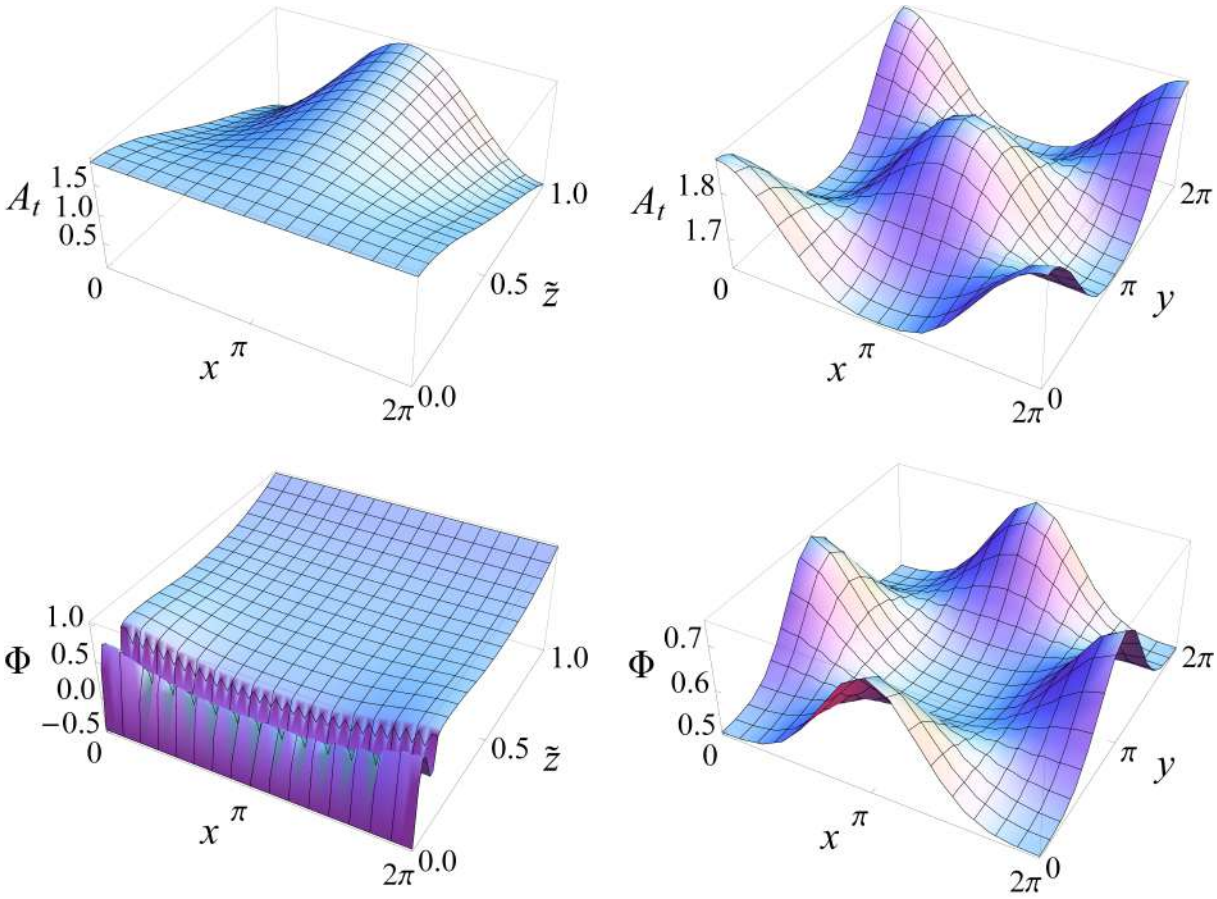

Figure 5.3: Numerically computed electrostatic (top) and dilaton (bottom) field along an x-$\tilde{z}$ slice at $y = 3.59$ (left) and along an x-y slice at $\tilde{z} = 0.22$ (right) for $\delta\mu = 1.0$ and $\alpha = -1.5$, with $\mu_0 = 1$, $\delta = 1$, $V_0 = 0.5$ and $T = 0.5$.

a propagation of the oscillatory behavior is actually in contrast with the observation of section 5.2 that the IR solutions satisfy the equations up to the half of the domain. Obviously, for the exact solutions to be revealed the sewing of the asymptotic solutions has to be highly nontrivial, although a comparison with [20] shows that our solutions exhibit good enough qualitative behavior, meaning that the functions $q_{\mu\nu}$ were indeed well chosen.

Yet, an interesting property of the dilaton solutions lies in the fact that the impact of the chemical potential on the bulk geometry actually depends on α. As we change α, Φ "oscillates" as a function of x and y, manifesting an effectively-dynamical behavior (since it resembles time-dependent fields). An inspection of the figures, and the other plots not shown here, shows that for $\alpha = -2$ the dilaton varies in space – roughly speaking – in phase with the electrostatic field, while the increment $\Delta\alpha = 0.5$ yields an approximate phase shift $\Delta x = \Delta y = \pi$ for $\alpha = -1.5$. We thus infer that Φ exhibits a kind of α-periodicity, although such a conclusion needs to be confirmed by a more involved analysis. However, the very fact that the overall profile of Φ actually depends on α implies that the IR geometry implicitly propagates all the way to the boundary, being thus even more dominant than we initially suggested in section 5.2.

effect which has emerged due to the discretization of the domain $\tilde{D}$ and, as such, may be ignored.

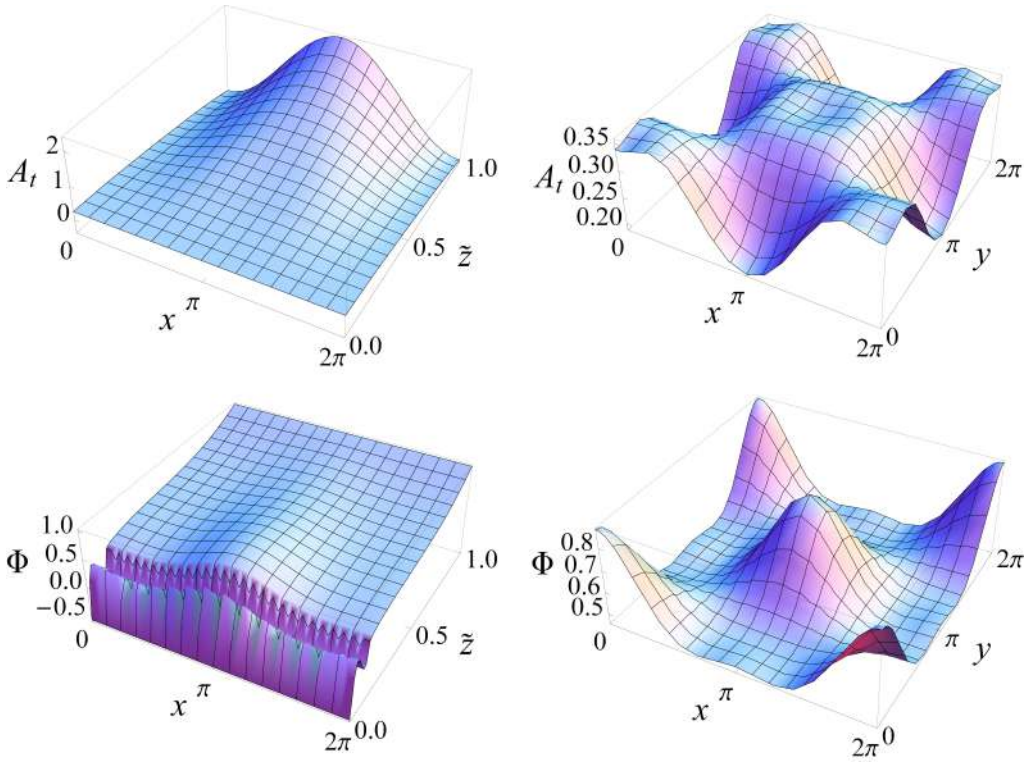

Figure 5.4: Numerically computed electrostatic (top) and dilaton (bottom) field along an x-$\tilde{z}$ slice at $y = 3.59$ (left) and along an x-y slice at $\tilde{z} = 0.22$ (right) for $\delta\mu = 1.5$ and $\alpha = -2.0$, with $\mu_0 = 1$, $\delta = 1$, $V_0 = 0.5$ and $T = 0.5$.

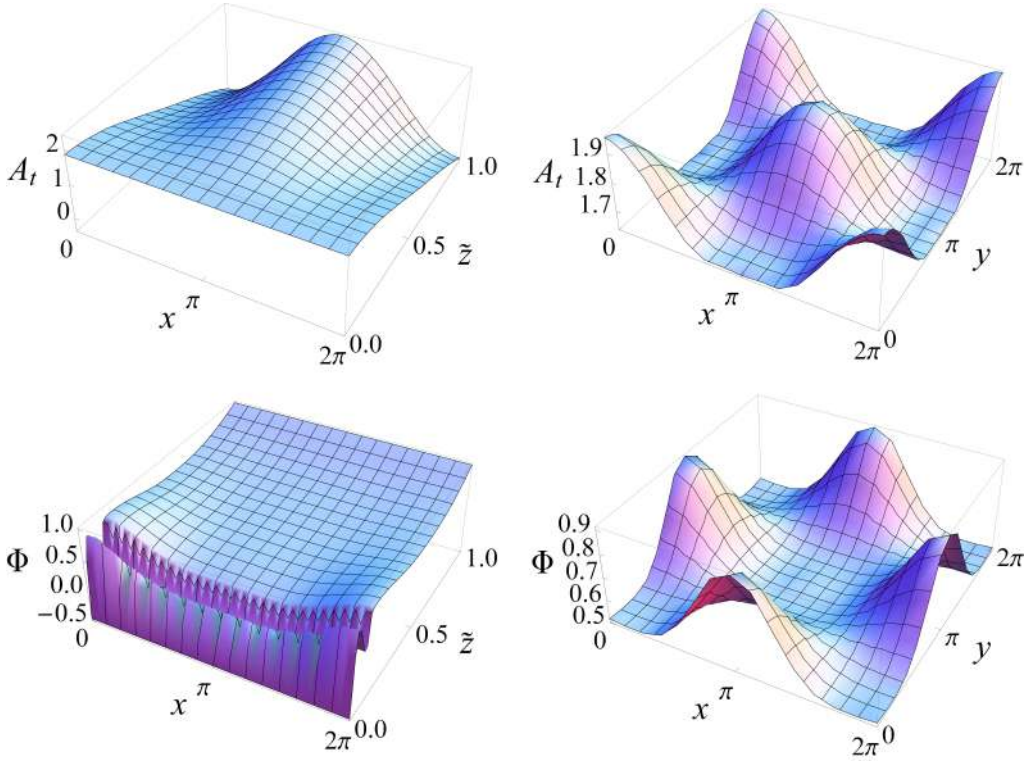

Figure 5.5: Numerically computed electrostatic (top) and dilaton (bottom) field along an x-$\tilde{z}$ slice at $y = 3.59$ (left) and along an x-y slice at $\tilde{z} = 0.22$ (right) for $\delta\mu = 1.5$ and $\alpha = -1.5$, with $\mu_0 = 1$, $\delta = 1$, $V_0 = 0.5$ and $T = 0.5$.

Chapter 6

Charge density and the Luttinger theorem

6.1 Holographic determination of the electric charge density

The preceding chapters were dedicated to a detailed analysis of the EMD equations and their solutions; eventually, we have found the solutions for the matter fields in an approximate hyperscaling-violating background. Now we are going to focus on the charge density and the Luttinger theorem as a concrete and simple indicator of the nature of the system.

In a quantum field theory the charge density is the expectation value of the charge density operator. It couples to the time component of the gauge field, so:

$$\rho = \frac{1}{i}\frac{\delta Z_{CFT}[\bar{A}_t]}{\delta \bar{A}_t}\Big|_{\bar{A}_t=0}, \tag{6.1}$$

where $\bar{A}_t$ is the electromagnetic scalar potential on the CFT side. Of course, we cannot take the functional derivative directly in field theory, since we do not know Z_{CFT} or $\bar{A}_t$, but we can use the GKPW formula, introduced in section 2.3. Switching to Euclidean time in order to simplify the generating functional of the bulk theory, we get

$$\rho = -\frac{\delta S_{bulk}}{\delta A_t}\Big|_{\tilde{z}=1}. \tag{6.2}$$

Another way to comprehend these relations is to recall that a generating functional in Euclidean coordinates represents the partition function. Since we work at finite density, the action will be equivalent to the grand canonical potential: $S_{bulk} = \beta\,\Omega[T,\mu]$, with $\beta = T^{-1}$ being equal to the integral over τ. Taking into account the classical thermodynamics, where the electric charge reads

$$\rho = -e\frac{\delta\Omega}{\delta\mu}, \tag{6.3}$$

and that the external electrostatic field is $A_t = \mu/e$, we reveal (6.2) again. We have restored the elementary charge e for the sake of easier dimensional analysis.

We now turn to the problem of our interest and vary the Euclidean EMD action (4.3) with respect to A_t:

$$\begin{aligned}\delta S_{bulk} &= -\int \mathrm{d}\tau \int \mathrm{d}^d x \int \mathrm{d}\tilde{z} \sqrt{g} Z(\Phi) F^{\mu\nu} \nabla_\mu \delta A_\nu = \\ &= -\int \mathrm{d}\tau \int \mathrm{d}^d x \int \mathrm{d}\tilde{z} \sqrt{g}\, \nabla_\mu (Z(\Phi) F^{\mu t} \delta A_t) = \\ &= -\int \mathrm{d}\tau \int \mathrm{d}^d x \sqrt{\gamma} Z(\Phi) n_\mu F^{\mu t} \delta A_t \big|_{\tilde{z}=1}. \end{aligned} \tag{6.4}$$

After integrating by parts, we have used the Maxwell equation (4.7) in the second line and the Stokes theorem in the third line, where γ and n are the determinant of the induced metric on the boundary and an outward pointing unit normal, respectively. The kinetic term of the electromagnetic field has the same sign as in the original action. This is because the zeroth component of the gauge field picks up a factor of i when Wick-rotated. Recalling the relation (6.2) and restoring the Lorentzian signature, we find[1]

$$\rho = -\sqrt{-\gamma} Z(\Phi) n_{\tilde{z}} F^{\tilde{z}t} \big|_{\tilde{z}=1}. \tag{6.5}$$

This relation holds quite generally: the differences stem only from the choice of Z, which in absence of a dilaton is just the usual coupling $1/e^2$. But Z aside, the right-hand-side of (6.5) is proportional to the electric field at the boundary, so we recognize a holographic version of Gauss-Ostrogradsky law.[2]

Once we have obtained numerical solutions for the matter fields, it is easy to compute the charge density. One has to use the already defined pseudospectral derivatives and evaluate (6.5) at every point of the numerical grid, along with insertion of the corresponding values for A_t and Φ.[3] Fixing $\tilde{z} = 1$ and selecting the remaining (x, y) subgrid, one obtains the desired result. An interpolation function is then easily constructed by the use of `Mathematica` and all quantities are readily found with analytical $\rho(x, y)$ at disposal.

A famous result which then relates the charge density to the Fermi surface in the case of Fermi liquids is the *Luttinger theorem*. The Luttinger theorem states that the d-dimensional volume enclosed by the Fermi surface is proportional to the electric charge density (averaged over the volume) to all orders in perturbation theory[4] [23, 22, 43]:

$$\frac{2e V_F^{(d)}}{(2\pi)^d} = \rho. \tag{6.6}$$

Crucially, the above expression knows nothing of the coupling strength or interactions in general – the density depends solely on the integral determined by the Fermi surface position. The Fermi surface is defined here as the locus of singularities of the logarithm of the Green's function: $\log G_R(0, \mathbf{k}_F) = \infty$. We can thus check if the holographic strange metal obeys the theorem by studying the dependence of ρ, if any, on the scaling exponents (as the proxy for the coupling strength), the lattice strength $\delta\mu/\mu_0$ and μ_0 itself. If the theorem holds we also obtain an estimate of the Fermi volume.

[1] Although we have used the $\tilde{z}$ coordinate because we continue with numerical calculations in the next section, the conclusions are valid for any choice of radial coordinate.

[2] Obviously, the electric flux must be constant through the bulk. This is the property of fractionalized geometry. Were we to include charged matter into the bulk, an additional flux would emerge, leading eventually to a modification of the Luttinger theorem [23].

[3] It is understood that we work in the approximate background.

[4] We have accounted for a double degeneracy due to the electron spin.

6.2 Numerical results

We now present and discuss the results obtained by the means of the holographic Gauss-Ostrogradsky law. We start from the ansatz (5.2) and find the induced metric on the boundary:

$$ds^2_{bdy} = \frac{r_h^2}{(1-\tilde{z}^2)^2}\left(-q_{tt}(x,y,\tilde{z})dt^2 + q_{xx}(x,y,\tilde{z})\left(dx^2+dy^2\right)\right), \tag{6.7}$$

and the outward pointing unit normal (as a one-form):

$$n = \frac{1}{1-\tilde{z}^2}\sqrt{\frac{4\tilde{z}^2 q_{\tilde{z}\tilde{z}}(x,y,\tilde{z})}{f(\tilde{z})} - \frac{2r_h^2 q^2_{x\tilde{z}}(x,y,\tilde{z})}{q_{xx}(x,y,\tilde{z})}}\,\mathrm{d}\tilde{z}. \tag{6.8}$$

Then we find the formula for the charge density using (6.5):

$$\begin{aligned}\rho(x,y) = Z(\Phi(x,y,\tilde{z}))&\sqrt{\frac{\tilde{z}^2 q_{\tilde{z}\tilde{z}}(x,y,\tilde{z})}{r_h^2 q_{tt}(x,y,\tilde{z})} - \frac{f(\tilde{z})q^2_{x\tilde{z}}(x,y,\tilde{z})}{2q_{tt}(x,y,\tilde{z})q_{xx}(x,y,\tilde{z})}}\times\\ &\times\left(Q\left(\frac{13+4\delta-\delta^2}{5+4\delta+\delta^2};x,y,\tilde{z}\right)\partial_x A_t(x,y,\tilde{z}) + \right.\\ &+ Q\left(\frac{28+6\delta-\delta^2}{10+6\delta+\delta^2};x,y,\tilde{z}\right)\partial_y A_t(x,y,\tilde{z}) -\\ &\left.\left. - \frac{q_{xx}(x,y,\tilde{z})}{q_{x\tilde{z}}(x,y,\tilde{z})}Q\left(\frac{49+8\delta-\delta^2}{17+8\delta+\delta^2};x,y,\tilde{z}\right)\partial_{\tilde{z}} A_t(x,y,\tilde{z})\right)\right|_{\tilde{z}=1},\end{aligned}$$

$$Q(\lambda;x,y,\tilde{z}) \equiv \left(\left(1-(1-\tilde{z}^2)^\lambda\right)\frac{q_{x\tilde{z}}(x,y,\tilde{z})}{q_{xx}(x,y,\tilde{z})} + \frac{2\tilde{z}^2 q_{\tilde{z}\tilde{z}}(x,y,\tilde{z})}{r_h^2 q_{x\tilde{z}}(x,y,\tilde{z})}\right)^{-1}. \tag{6.9}$$

In order to get numerical values for $\rho \equiv \langle\rho(x,y)\rangle$ as described in the previous section, we employ again the ansätze (5.8–5.11) for the functions $q_{\mu\nu}$. The results are given in Tables 6.1 and 6.2 and Figures 6.1–6.3. The actual numerical values are not important for our story; we give them in the tables just for completeness.

$\delta\mu\backslash\alpha$	-2.3	-2.1	-1.9	-1.7	-1.5
0.5	4.88	3.50	2.29	0.87	-2.33
1.0	5.14	3.66	2.38	0.90	-2.41
1.5	5.61	3.97	2.55	0.95	-2.55

Table 6.1: The charge density ρ for three values of the lattice amplitude $\delta\mu$ (in units of the average chemical potential μ_0) and different values of the EMD parameter α, with $\mu_0 = 1$, $\delta = 1$, $V_0 = 0.5$ and $T = 0.5$.

Figure 6.1 shows the dependence of the charge density on α for the three ratios $\delta\mu/\mu_0$ examined in the previous chapter. If our system were a Fermi liquid, its charge density would know nothing about the IR scaling. It would be constant because of the unbroken U(1) symmetry, which leads to the corresponding Ward-Takahashi identity implying charge conservation. Obviously, this is not the case – whatever the strength of the modulation $\delta\mu$ is, ρ decreases with α. Since the critical exponents increase monotonically with

$\alpha\backslash\mu_0$	0.5	0.6	0.7	0.8	0.9	1.0	1.1	1.2	1.3	1.4	1.5
-2.3	1.96	2.53	3.12	3.75	4.42	5.14	5.93	6.78	7.71	8.70	9.61
-1.7	-0.56	-0.27	0.01	0.30	0.60	0.90	1.21	1.53	1.87	2.24	2.62
-1.5	-3.95	-3.62	-3.30	-2.99	-2.69	-2.41	-2.12	-1.85	-1.57	-1.30	-1.03

Table 6.2: The charge density ρ for three values of the EMD parameter α and different values of the average chemical potential μ_0, with fixed relative lattice strength $\delta\mu/\mu_0 = 1$, and $\delta = 1$, $V_0 = 0.5$, $T = 0.5$.

α for fixed δ, ρ decreases with θ and $\mathbf{z}$ too. We thus recognize a true non-Fermi-liquid behavior. Had we found the charge density to be α-independent, the next step would be to solve the Dirac equation for the probe fermion and to determine its spectrum; the Green's function would give us the position of the Fermi surface, and we would be able to compute the Fermi volume and check the prediction of the Luttinger theorem. Since we have found a non-Fermi liquid instead, the relation (6.6) certainly does not hold and there is no need to check it further by determining $\mathbf{k}_F$ from the spectrum. Nevertheless, the fermionic spectra are thoroughly studied in [20] both for their own sake and for comparison with the QMC simulations of the Hubbard model. The spectra from [20] confirm the existence of various non-Fermi-liquid phases, with asymmetric quasiparticle peaks or with no quasiparticle peaks at all.

The fact that the three curves in Figure 6.1 almost coincide implies relative insensitivity of the system to the amplitude of the lattice, meaning that in this respect weak and strong lattices do not differ much. Interestingly, it seems that for $\alpha > -1.7$ the charge densities "exchange the roles" regarding their magnitudes, maintaining the order with respect to their absolute value.

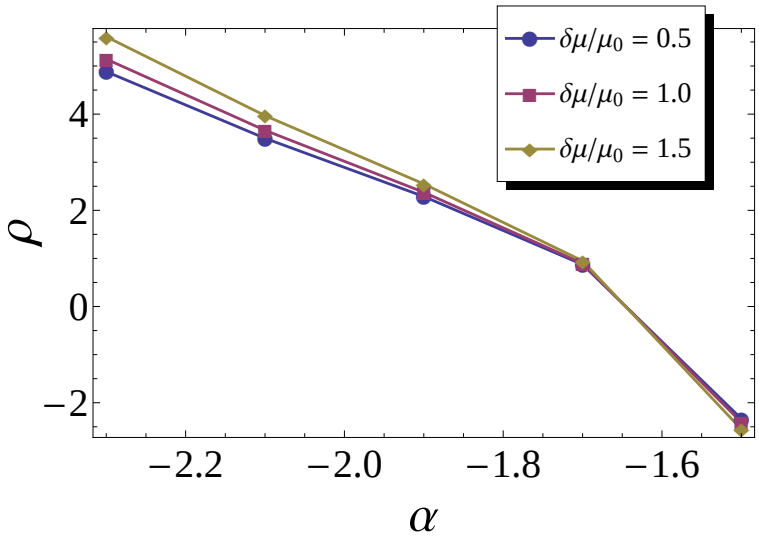

Figure 6.1: The charge density as a function of the EMD parameter α for three values of the relative lattice strength $\delta\mu/\mu_0$, with $\mu_0 = 1$, $\delta = 1$, $V_0 = 0.5$ and $T = 0.5$. The charge density is strongly dependent on α, hence the Luttinger theorem is not satisfied.

Another interesting insight into the properties of our strange metal is offered by the μ_0-dependence of ρ, given in Figure 6.2 for three values of α. As expected, the charge density increases with doping, exhibiting even a transition between an overdoped and underdoped

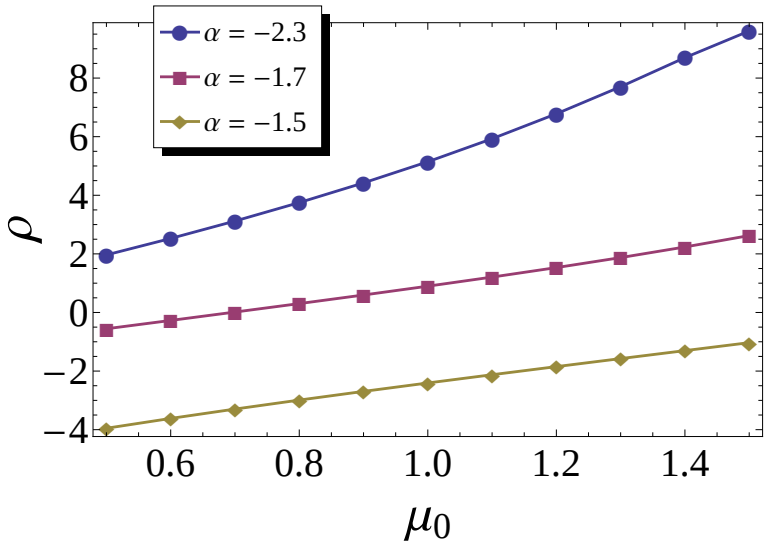

Figure 6.2: The charge density as a function of the average chemical potential μ_0 for three values of α and fixed ratio $\delta\mu/\mu_0 = 1$, with $\delta = 1$, $V_0 = 0.5$ and $T = 0.5$.

material in the case of $\alpha = -1.7$. The increase is approximately linear (except to some extent for $\alpha = -2.3$) and we recognize a typical metallic behavior (usually observed in strange metals too), at least for the domain of the EMD parameters we have examined. What we expect but do not see is the saturation of charge density for some chemical potential ("Mott Plateau"), which is normally seen in the Hubbard model [10]. Of course, it might simply happen for the values of μ_0 or α that we have not checked explicitly. One might still find the saturation upon the extension of the domain for μ_0.

Finally, we plot the spatial distribution of the charge density in Figure 6.3. The distribution is periodic as it has to be, but what is somewhat striking is its strong delocalization, which implies that we indeed deal with a metallic phase (although apparently strange) rather than a Mott-like system with (almost) localized or quenched charges.

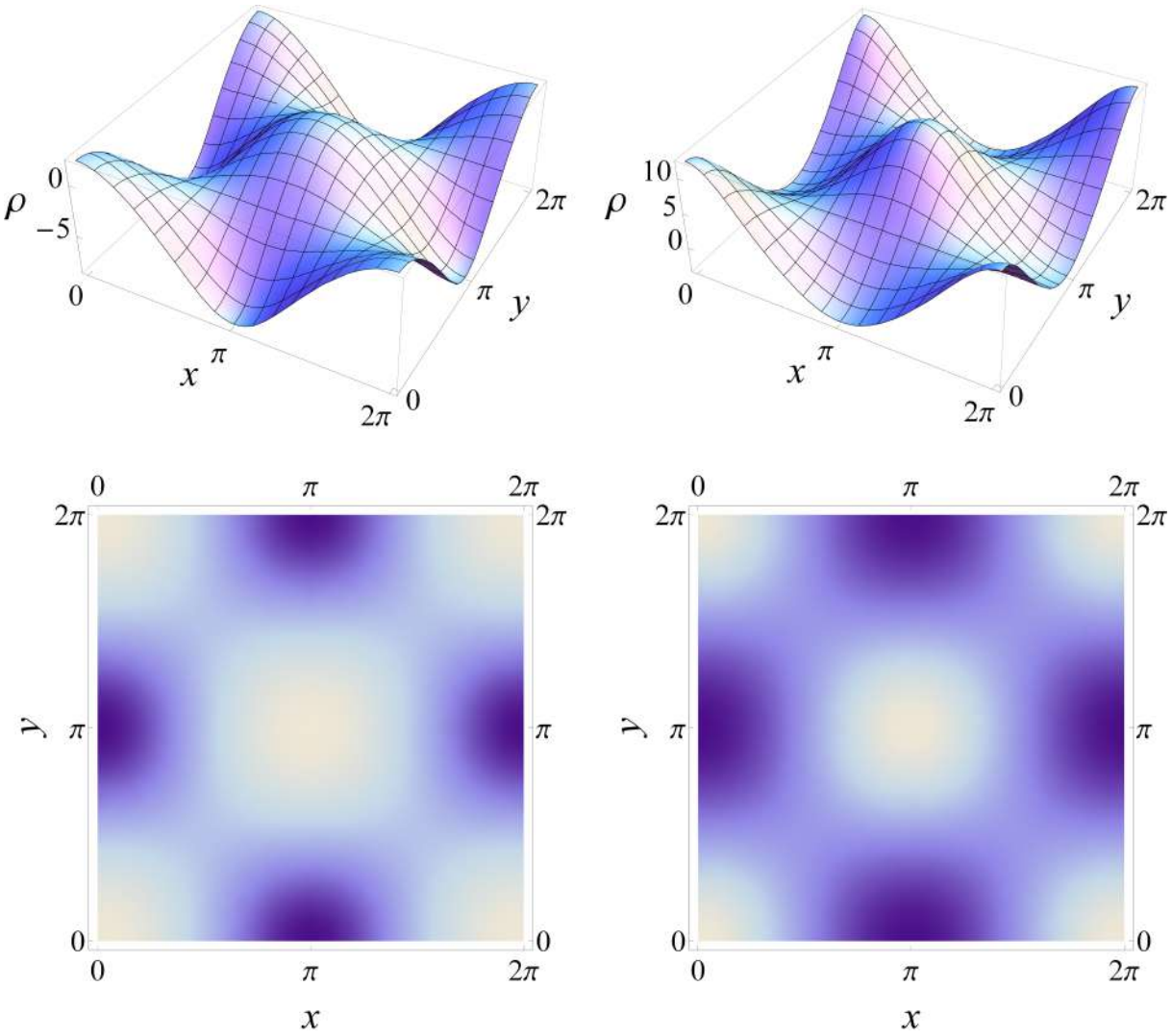

Figure 6.3: 3D plots (top) and density plots (bottom) of the charge density $\rho(x, y)$ for $\alpha = -1.5$ (left) and $\alpha = -2.0$ (right), with $\mu_0 = 1$, $\delta\mu = 1.5$, $\delta = 1$, $V_0 = 0.5$ and $T = 0.5$. The top and bottom row show exactly the same data. The charge density is strongly delocalized and distributed all over the unit cell.

Chapter 7

Discussion and conclusions

The results of this thesis confirm our overall success in constructing the holographic dual of a strongly coupled field theory. However, we have comprehended only a small portion of the phenomenology pertaining to the square lattice. It may be said that we have actually inspected a "necessary condition" for existence of a non-Fermi liquid, manifested as the α-dependence of the charge density. A natural "sufficient condition" would then be offered by the fermionic Green's functions. The analysis of the fermionic spectra in [20] in general confirms the conclusions of this thesis, but by no means gives a definitive characterization of the holographic strange metal. We are still at the beginning of the conquest of this topic. Importantly, all the insights gained through the examination of both the "sufficient" and "necessary" conditions rest on phenomenology. It is certainly very rich, but we would like the AdS/CFT correspondence to give us also some novel theoretical knowledge regarding the underlying physics of strange metals. Conversely, we hope that every step forward in AdS/CMT, with the holographic 2D lattice not being the least, might eventually lead to a better understanding of both the correspondence itself (especially in the bottom-up approach) and the fundamental laws of nature explained thereof.

We are, of course, far from comprehending these issues. We have mentioned them only in order to illustrate the place of our work in the contexts of holography and condensed matter, and to mark the ultimate goal we are striving for. The next step we are going to make in our research is still tightly related to the results presented in this thesis. In the first place, we would like to solve the whole system of the EMD equations and check whether the above conclusions still hold. Besides, we would like to examine a wider domain of parameters, and thus to get a more complete insight into the behavior of the charge density. On the other hand, we are particularly interested in properties of the dilaton, because of its peculiar response to the chemical potential; also, we are interested in the physical meaning of its dual (scalar) operator.

Bibliography

[1] A A Abrikosov, I Dzyaloshinskii, L P Gorkov, and Richard A Silverman. *Methods of quantum field theory in statistical physics*. Dover, New York, NY, 1975.

[2] P. Nozières and David Pines. *The theory of quantum liquids*. Perseus Books,, Cambridge, 1999. Includes bibliographical references and index..

[3] Nabil Iqbal, Hong Liu, and Márk Mezei. Lectures on holographic non-fermi liquids and quantum phase transitions. 10 2011.

[4] Subir Sachdev and Bernhard Keimer. Quantum criticality. *Physics Today*, 64(2):29–35, feb 2011.

[5] C P Herzog. Lectures on holographic superfluidity and superconductivity. *Journal of Physics A: Mathematical and Theoretical*, 42(34):343001, aug 2009.

[6] Hilbert v. Löhneysen, Achim Rosch, Matthias Vojta, and Peter Wölfle. Fermi-liquid instabilities at magnetic quantum phase transitions. *Rev. Mod. Phys.*, 79:1015–1075, Aug 2007.

[7] Philipp Gegenwart, Qimiao Si, and Frank Steglich. Quantum criticality in heavy-fermion metals. *Nature Physics*, 4(3):186–197, mar 2008.

[8] Richard L. Greene, Pampa R. Mandal, Nicholas R. Poniatowski, and Tarapada Sarkar. The strange metal state of the electron-doped cuprates. *Annual Review of Condensed Matter Physics*, 11(1):213–229, mar 2020.

[9] Philip W. Phillips, Nigel E. Hussey, and Peter Abbamonte. Stranger than metals, 2022.

[10] Richard T. Scalettar. 4 an introduction to the hubbard hamiltonian. 2016.

[11] J. P. F. LeBlanc, Andrey E. Antipov, Federico Becca, Ireneusz W. Bulik, Garnet Kin-Lic Chan, Chia-Min Chung, Youjin Deng, Michel Ferrero, Thomas M. Henderson, Carlos A. Jiménez-Hoyos, E. Kozik, Xuan-Wen Liu, Andrew J. Millis, N. V. Prokof'ev, Mingpu Qin, Gustavo E. Scuseria, Hao Shi, B. V. Svistunov, Luca F. Tocchio, I. S. Tupitsyn, Steven R. White, Shiwei Zhang, Bo-Xiao Zheng, Zhenyue Zhu, and Emanuel Gull. Solutions of the two-dimensional hubbard model: Benchmarks and results from a wide range of numerical algorithms. *Phys. Rev. X*, 5:041041, Dec 2015.

[12] Emanuel Gull, Andrew J. Millis, Alexander I. Lichtenstein, Alexey N. Rubtsov, Matthias Troyer, and Philipp Werner. Continuous-time monte carlo methods for quantum impurity models. *Rev. Mod. Phys.*, 83:349–404, May 2011.

[13] Antoine Georges, Gabriel Kotliar, Werner Krauth, and Marcelo J. Rozenberg. Dynamical mean-field theory of strongly correlated fermion systems and the limit of infinite dimensions. *Rev. Mod. Phys.*, 68:13–125, Jan 1996.

[14] G. Rohringer, H. Hafermann, A. Toschi, A. A. Katanin, A. E. Antipov, M. I. Katsnelson, A. I. Lichtenstein, A. N. Rubtsov, and K. Held. Diagrammatic routes to nonlocal correlations beyond dynamical mean field theory. *Rev. Mod. Phys.*, 90:025003, May 2018.

[15] Jan Zaanen, Ya-Wen Sun, Yan Liu, and Koenraad Schalm. *Holographic Duality in Condensed Matter Physics*. Cambridge Univ. Press, 2015.

[16] Juan Martin Maldacena. The Large N limit of superconformal field theories and supergravity. *Adv. Theor. Math. Phys.*, 2:231–252, 1998.

[17] S. S. Gubser, Igor R. Klebanov, and Alexander M. Polyakov. Gauge theory correlators from noncritical string theory. *Phys. Lett. B*, 428:105–114, 1998.

[18] Edward Witten. Anti-de Sitter space and holography. *Adv. Theor. Math. Phys.*, 2:253–291, 1998.

[19] Sean A. Hartnoll, Andrew Lucas, and Subir Sachdev. Holographic quantum matter, 2016.

[20] Filip Herček, Vladan Gecin, and Mihailo Čubrović. Photoemission "experiments" on holographic lattices, 2022.

[21] Aristomenis Donos, Jerome P. Gauntlett, and Vaios Ziogas. Diffusion for Holographic Lattices. *JHEP*, 03:056, 2018.

[22] G. D. Mahan. *Many Particle Physics, Third Edition*. Plenum, New York, 2000.

[23] Nabil Iqbal and Hong Liu. Luttinger's theorem, superfluid vortices and holography. *Classical and Quantum Gravity*, 29(19):194004, aug 2012.

[24] Juan Martin Maldacena. TASI 2003 lectures on AdS / CFT. In *Theoretical Advanced Study Institute in Elementary Particle Physics (TASI 2003): Recent Trends in String Theory*, pages 155–203, 9 2003.

[25] Torben Skrzypek and Jannik Fehre. Introduction to conformal field theory. 2018.

[26] Joshua D. Qualls. Lectures on conformal field theory, 2015.

[27] David Tong. *Gauge Theory*. 2018.

[28] G. 't Hooft. Large N. In *The Phenomenology of Large N(c) QCD*, pages 3–18, 4 2002.

[29] Aron C. Wall. A Survey of Black Hole Thermodynamics. 4 2018.

[30] James M. Bardeen, B. Carter, and S. W. Hawking. The Four laws of black hole mechanics. *Commun. Math. Phys.*, 31:161–170, 1973.

[31] S. W. Hawking. Particle Creation by Black Holes. *Commun. Math. Phys.*, 43:199–220, 1975. [Erratum: Commun.Math.Phys. 46, 206 (1976)].

[32] G. W. Gibbons and S. W. Hawking, editors. *Euclidean quantum gravity*. 1994.

[33] S. Carlip. Black Hole Thermodynamics. *Int. J. Mod. Phys. D*, 23:1430023, 2014.

[34] Daniel Z. Freedman, Samir D. Mathur, Alec Matusis, and Leonardo Rastelli. Correlation functions in the CFT/AdS correspondence. *Nuclear Physics B*, 546(1-2):96–118, apr 1999.

[35] Thomas Faulkner, Hong Liu, John McGreevy, and David Vegh. Emergent quantum criticality, Fermi surfaces, and AdS(2). *Phys. Rev. D*, 83:125002, 2011.

[36] Norihiro Iizuka, Nilay Kundu, Prithvi Narayan, and Sandip P. Trivedi. Holographic fermi and non-fermi liquids with transitions in dilaton gravity. *Journal of High Energy Physics*, 2012(1), jan 2012.

[37] Tomas Andrade, Alexander Krikun, Koenraad Schalm, and Jan Zaanen. Doping the holographic mott insulator. *Nature Physics*, 14(10):1049–1055, jul 2018.

[38] Markus Heusler. *Black hole uniqueness theorems*. Cambridge lecture notes in physics 6. Cambridge University Press, 1996.

[39] Tomas Andrade. Holographic lattices and numerical techniques, 2017.

[40] Alexander Krikun. Numerical solution of the boundary value problems for partial differential equations. crash course for holographer, 2018.

[41] Conor Joseph McCoid. Spectral differentiation: Integration and inversion, 2015.

[42] Matthew Headrick. diffgeo.m. http://people.brandeis.edu/~headrick/Mathematica/, 2015.

[43] Joshuah T Heath and Kevin S Bedell. Necessary and sufficient conditions for the validity of luttinger's theorem. *New Journal of Physics*, 22(6):063011, jun 2020.